

Evidence of Intermittent Cascades from Discrete Hierarchical Dissipation in Turbulence

Wei-Xing Zhou¹ and Didier Sornette^{1,2,3}

1. Institute of Geophysics and Planetary Physics, University of California, Los Angeles, CA 90095
2. Department of Earth and Space Sciences, University of California, Los Angeles, CA 90095
3. Laboratoire de Physique de la Matière Condensée, CNRS UMR 6622 and Université de Nice-Sophia Antipolis, 06108 Nice Cedex 2, France

Abstract

We present the results of a search of log-periodic corrections to scaling in the moments of the energy dissipation rate in experiments at high Reynolds number (≈ 2500) of three-dimensional fully developed turbulence. A simple dynamical representation of the Richardson-Kolmogorov cartoon of a cascade shows that standard averaging techniques erase by their very construction the possible existence of log-periodic corrections to scaling associated with a discrete hierarchy. To remedy this drawback, we introduce a novel “canonical” averaging that we test extensively on synthetic examples constructed to mimick the interplay between a weak log-periodic component and rather strong multiplicative and phase noises. Our extensive tests confirm the remarkable observation of statistically significant log-periodic corrections to scaling, with a preferred scaling ratio for length scales compatible with the value $\gamma = 2$. A strong confirmation of this result is provided by the identification of up to 5 harmonics of the fundamental log-periodic undulations, associated with up to 5 levels of the underlying hierarchical dynamical structure. A natural interpretation of our results is that the Richardson-Kolmogorov mental picture of a cascade becomes a realistic description if one allows for intermittent births and deaths of discrete cascades at varying scales.

1 Introduction

Since Kolmogorov’s presentation of his theory of three-dimensional fully developed turbulence in 1941 (see [13] for a modern account), there has been a vigorous continuing investigation aimed at verifying its accuracy and testing for possible deviations. While its main predictions ($k^{-5/3}$ spectrum of velocity fluctuations, universality of the exponents of structure functions in the inertial range) are verified to a good approximation, there are clear deviations. The most notable is the nonlinear dependence of the exponents ζ_q of the structure functions as a function of their order q , which is a hallmark of multifractality [35]. There is also a strong interest in testing Kolmogorov’s universality assumptions that all the small-scale statistical properties are uniquely and universally determined by the scale ℓ , the mean energy dissipation rate $\bar{\epsilon}$ and the viscosity (see [38] for recent evidence of the contrary) and that there is a well-defined limit at infinite Reynolds number (see [4, 10, 48] for alternative scenarios).

Kolmogorov’s K41 hypotheses “were based physically on Richardson’s idea [39] of the existence in the turbulence flow of vortices of all possible scales...” [27] and turbulence phenomenology is often cast in terms of a cartoon depicting a cascade of the energy introduced into the largest eddies

of size ℓ_0 and “cascading” down a hierarchy of eddies of size $\ell_n = \ell_0/\gamma^n$ where $\gamma > 1$ (often taken equal to 2 but without particular significance: [13] bottom of page 103) at the same rate ϵ and being eventually removed by dissipation at the smallest scales. To our knowledge, Novikov was the first to point out in 1966 that, if the discrete hierarchy of the cascade is taken seriously with a specific γ , the structure functions in turbulence should contain log-periodic oscillations [33, 34]. His argument was that, if an unstable eddy in a turbulent flow typically breaks up into smaller eddies of about half or a third of its size ($\gamma = 2$ or 3), but not into eddies ten or twenty times smaller, then one can suspect the existence of a preferred scale factor γ , hence the log-periodic oscillations. Smith et al. [43] confirmed on explicit geometrical examples involving generalizations of the triadic Cantor set that log-periodic corrections to scaling arise in fractal models with lacunarity, i.e., having a preferred scaling ratio γ between scales. Shell models construct explicitly a discrete scale invariant set of equations on a hierarchy of shells $k_n = 2^n k_0$ in momentum space whose solutions are marred by unwanted log-periodicities (see for instance [31] for a refinement addressing the problem).

Oscillations in log-log plots of structure functions and other quantities are often observed but do not seem to be stable and depend on the nature of the global geometry of the flow and recirculation [13, 2] as well as the analyzing procedure. In his book ([13], pages 130-131), Frisch discusses the possible existence of such log-periodic corrections and points out that the “extended self-similarity” technique [5] which has significantly improved the accuracy of exponents may be useful in particular because it overcomes the distortions stemming from the undulations which appear to be correlated across the different orders of structure functions (see Appendix B).

Hints of the presence of log-periodic undulations decorating the power laws can be observed in Fig. 8 of Ref. [32] which studied the multifractal nature of turbulent energy dissipation, in Fig. 5.1 p.58 and Fig. 8.6 p.128 of Ref. [13], Fig. 3.16 p.76 of Ref. [3], Fig. 1b of Ref. [51] and Fig. 2b of Ref. [9] (to list a few). However, these barely perceptible undulations are far from proving the existence of a genuine discrete hierarchical cascade in three-dimensional flows, a la Richardson-Kolmogorov, as they are in general considered as “noise”. Furthermore, if it exists, the scale ratio γ has not been constrained.

A preliminary attempt has dealt with another type of turbulence, namely freely decaying 2-D turbulence [26], in which experimental evidence and theoretical arguments suggest that the time-evolution of freely decaying 2-D turbulence is governed by a discrete time scale invariance rather than a continuous time scale invariance. The number of vortices, their radius and their separation display log-periodic oscillations as a function of time with an average log-frequency of $\sim 4 - 5$ corresponding to a preferred scaling ratio of $\sim 1.2 - 1.3$. Since the statistical significance for each data set taken separately is not good when comparing with a large variety of different stochastic processes taken as null-hypothesis [53], Ref. [26] argued about a good statistical significance of this log-periodic oscillations on the basis of the coincidence of three highest peaks of the periodogram analysis which occur at log-frequencies far from the most probable frequencies occurring solely from noise. An alternative possibility is that the log-periodicity results from the long-range correlations in fractional Gaussian like-noise with Hurst exponent of the order of $H \approx 0.3$. This case stresses the difficulty and complication of determination of the significance level of a log-periodic signal.

The theory and practice of log-periodicity and its associated complex exponents has advanced significantly in the last few years [47, 30]. It has become clear in the 1980s that complex exponents and log-periodicity appears as soon as a given physical problem is formulated on a discretely hierarchical geometry or network. More interestingly, only recently has it been realized that discrete scale invariance (DSI) and its associated complex exponents may appear “spontaneously” in Euclidean systems [41], i.e., without the need for a pre-existing geometrical hierarchy. Systems

where self-organized DSI has been reported include Laplacian growth models [45, 17], rupture in heterogeneous systems [1, 23], earthquakes [44, 40, 20, 25, 19], animals [41], biased diffusion in percolating systems [50] as well as in financial time series preceding crashes [22, 24, 11, 49]. In addition, general field theoretical arguments [41] indicate that complex exponents are to be expected generically for out-of-equilibrium and/or quenched disordered systems. This together with Novikov’s argument suggest to revisit log-periodicity in turbulent signals. Demonstrating unambiguously the presence of log-periodicity and thus of DSI in turbulent time-series would provide an important step towards a direct demonstration of the Richardson-Kolmogorov cascade or at least of its hierarchical imprint.

The present paper presents the results of such an investigation on the log-periodic oscillations of the energy dissipation rate in 3-dimensional fully developed turbulence. In section 2, we explain where lie the difficulties of this enterprise and what are the classical traps of standard averaging methods. We stress in particular that standard ensemble averaging destroy the putative log-periodic undulations in the limit of large sample sizes. To address this problem, we explain our new “canonical” averaging methodology for extracting a possible log-periodic signal in turbulence time series and test it on synthetic examples. In section 3, we present the result of our analysis for different orders of the moments of the energy dissipation rate. In particular, we discuss the sensitivity of the results with respect to the filtering parameters of our technique. Appendix A presents a study of the dependence of the bandwidth selectivity of the Savitsky-Golay filter as a function of its parameters M (order of polynomial fit) and $2N_L + 1$ (number of points) using the smoothing procedure. Appendix B proposes a simple multifractal model accounting for the observation that the same set of log-frequencies, within numerical accuracy, are found independently of the moment orders varying from $q = 1$ to 19.

2 “Canonical” averaging of undulations with noisy phases

2.1 Characterization of the effect of averaging on the detection of log-periodicity

If discrete scale invariance (DSI) exists in turbulence, this should be reflected in the existence of a hierarchy of characteristic scales $\ell, \ell/\gamma, \ell/\gamma^2, \dots$ where γ is a preferred scaling ratio and ℓ is a macroscopic scale.

Actually, this naive picture has to be revised to account for dynamical effects. If it exists, let us imagine that the energy cascade starts over some region at some instant from some scale ℓ_a and then proceeds down the scales over a few generations of the hierarchy. It will probably be interrupted by various competing processes that break down the localness of the interactions due for instance to the influence of very thin shear layers [28] or slender vortex filaments [29, 8]. Later, at another time in some other region, another energy cascade may start from some other scale ℓ_b and then proceeds downwards over a different number of generations of the hierarchy. If this picture has some element of truth, there is an immediate consequence with respect to the detectability of log-periodicity associated with these transient cascades:

1. such log-periodic undulations will be transient in a long time series;
2. different burst of log-periodic oscillations will have different phases.

Indeed, consider a pure log-periodic signal

$$S(r) = \cos(2\pi f \ln r - \psi_a) \tag{1}$$

of a structure function or moment as a function of scale r , where

$$f = 1/\ln \gamma \quad (2)$$

is the log-frequency. The phase ψ_a can be redefined as $\psi_a = 2\pi f \ln \ell_a$ such that the undulation becomes $\cos(2\pi f \ln(r/\ell_a))$. The values $r_0 = \ell_a, r_1 = \ell_a/\gamma, r_2 = \ell_a/\gamma^2, \dots$ of the scale r corresponding to the maxima of the cosine function provide the discrete scales of the underlying cascade, which are all proportional to the “root” length scale ℓ_a . If a second cascade is triggered from a slightly different scale ℓ_b , the resulting oscillation $\cos(2\pi f \ln r - \psi_b)$ with the same log-frequency will be out-of-phase compared to the first one with a phase shift $\psi_a - \psi_b = 2\pi f \ln(\ell_a/\ell_b)$. This scenario suggests that, while the physics of the cascade may be universal with an universal scaling factor γ , the phases are sensitively dependent on the specific scale from which a given transient cascade nucleates. As the cascade may be dynamically triggered from a variety of scales ℓ_a from the integral scale and deep in the inertial range, the corresponding phases are expected to be non-universal. Averaging a signal over several such transient cascades will thus wash out the information by “destructive interferences” of the log-periodic oscillations, giving them the appearance of noise.

A similar situation has already been documented in other systems. Numerical simulations on Laplacian growth models [45, 17, 21] and renormalization group calculations [41] have taught us that the presence of noise or disorder modifies the phase in the log-periodic oscillations in a sample specific way leading to a “destructive interference” upon averaging. As sample-to-sample log-periodic undulations are destroyed by averaging over a long record, this is related to the self-averaging property [7, 36, 52].

2.2 Existing methods for detecting log-periodicity

Up to now, four different methods have attempted to improve on standard averaging techniques which, in our context, may “throw away the baby with the bath”.

1. A first method consists in fitting data with a power law decorated by the log-periodic corrections as done to improve the determination of the time of occurrence of rupture [1, 23], of earthquakes [44, 40, 20, 25] and of financial crashes [46, 22, 24, 49]. This parametric approach has the drawback of becoming unstable when too much noise is present.
2. The second idea is to avoid performing any average altogether and, studying the main log-frequency of each realization, to construct their distribution over the whole set of realizations. This was used in an early attempt to demonstrate the presence of DSI structure in growing diffusion-limited-aggregation clusters [20].
3. The third non-parametric approach uses the fact that a periodogram obtained with the Lomb method [37] (see also below for more details) gives the power spectrum as a function of log-frequency independently of the phase of the undulations. As a consequence, if there is a genuine peak, even with a lot of noise, performing a Lomb periodogram for each sample and then averaging the Lomb periodograms will tend to make the genuine peak stand out of the noise if there are sufficiently many independent samples. This is the method used for the analysis of 2-D freely decaying turbulence [26] already mentioned.
4. Ref. [21] have adapted to the problem of log-periodic oscillation the novel so-called “canonical” averaging scheme proposed in [36] based on the determination of a realization-dependent effective critical point obtained from, *e.g.*, a maximum susceptibility criterion. Conceptually,

the method re-sets the nucleus scale ℓ_a of the cascade in different realizations to approximately the same value and then only afterwards perform the averaging. The non-parametric method has been tested successfully on diffusion limited aggregation clusters and on a model of rupture [21]. For the problem of diffusion-limited aggregation, “canonical” averaging amounts to average at fixed numbers of particles per cluster. In the rupture problem, a maximum rate of released energy is used to determine the position of the realization-specific critical control parameter which is then used to perform an average over many different realizations at fixed reduced distance from the critical rupture. Ref. [48] suggested to adapt this idea to turbulence by dividing a long turbulence time series into intervals of length equal to a turn-over time and rephasing the structure functions estimated over each such time interval by identifying a scale at which the dissipation rate is locally the largest.

2.3 Our new improved “canonical” averaging procedure

Here, we present a novel extension of the fourth method that turns out to perform extremely well. We now describe and illustrate it on simple synthetic data before turning to the full-fledge analysis of a long turbulent time series. Since our goal is to detect log-periodicity in the structure function for which the natural variable is the logarithm of the scale, we can rephrase the problem into one of detecting a periodic undulation in a noisy time series.

Consider for the sake of presentation, a signal similar to (1). Posing $t \equiv \ln r$, we have the following “time” series

$$y(t) = \cos(2\pi ft + \psi(t)) , \quad (3)$$

where the phase $\psi(t)$ is now time varying to account for the variation of the scale of the nucleus of the cascade described above. Here, we do not show tests with additive noise as this standard situation was studied in [37, 18] and is relatively easily addressed with the Lomb periodogram spectral analysis (see also below). We thus focus our attention on the most difficult situation of random phases.

To be specific, let us assume that $\psi(t)$ undergoes a random walk

$$\psi(t) = \psi(t - dt) + 2\pi\sqrt{f} A \text{ran}(t) , \quad (4)$$

where $\text{ran}(t)$ is a Gaussian random number of zero mean and of variance dt . With this parameterization (4), over N periods $1/f$ of the deterministic component, the phase wanders by an amplitude of the order of $2\pi A\sqrt{N}$ which is rapidly larger than 2π if A is comparable to 1 as we discuss here. This random phase modulation can also be seen as a multiplicative noise acting on the signal $(\cos(2\pi ft), \sin(2\pi ft))$ in the complex plane since $\cos(2\pi ft + \psi(t)) = \cos \psi \cos(2\pi ft) - \sin \psi \sin(2\pi ft)$. In the absence of the deterministic signal $2\pi ft$ in the cosine in expression (3), the random process $y(t)$ has a correlation function which can be evaluated exactly: $\langle \cos(\psi(t + \tau)) \cos(\psi(t)) \rangle - \langle \cos(\psi(t + \tau)) \rangle \langle \cos(\psi(t)) \rangle = e^{-2\pi^2 A^2 \tau}$ with a characteristic correlation time $1/2\pi^2 A^2$.

Figure 1 shows one realization with 100 points of the time series (3,4) with $f = 1, A = 0.3$ generated numerically with $dt = 0.1$ in the time interval $[0, 10]$. This corresponds to a correlation time $1/2\pi^2 A^2 = 0.44$. This value $A = 0.3$ thus corresponds to a very strong phase disorder, so strong that the time series appears very random. Figure 2 shows a standard spectral analysis (Fourier spectrum) of a long time series with 2000 points in the time interval $[0, 200]$. It is clear that the random walk of the phase $\psi(t)$ destroys completely the information of the existence of an underlying deterministic component at the frequency $f = 1$: the figure shows a completely noisy spectrum.

Figure 3 shows the result of the third method listed in section 2.2: we take the long time series with 2000 points in the time interval $[0, 200]$ and divide it in 20 contiguous time series of 100 points each that are similar to that represented in Fig. 1. We perform on each of these 20 time series a Lomb periodogram analysis and then average these 20 Lomb periodograms. The Lomb periodogram analysis performs local least-square fits of the data by sinusoids centered on each data point of the time series [42]. The Lomb periodogram usually out-performs significantly other spectral methods for unevenly sampled and relatively short signals [42, 16, 37, 53]. Figure 3 provides already a significant improvement over the standard Fourier analysis of Fig. 2, as a quite broad but rather clear peak centered approximately on $f = 1$ can be distinguished. However, its statistical significance is not convincing since the hypothesis that it could result just from random occurrences can not be rejected by standard statistical tests [37, 53].

Our new method consists in the following steps.

1. Rather than analyzing the long time series of 2000 points, we divide it again in 20 contiguous time series of 100 points each: $[1, 100]$; $[101, 200]$; ... $[1+n \times 100, (n+1) \times 100]$; ...; $[1901, 2000]$. These two numbers 20 and 100 are rather arbitrary and can be modified by and large. We need however a sufficient number of times series to average over as discussed below and a sufficient number of points in each time series to carry at least a few oscillations.
2. On each sub-time series of 100 points, we apply the Savitsky-Golay filter [37] over a running window of size $N_L + N_R + 1$ (with N_L points to the left and N_R points to the right of a running point) by fitting a polynomial of order M . We take $N_L = N_R$ (symmetric filter) and vary N_L between 5 and 10 and M between 4 and 7, both by unit increments. This provides a total of 24 filtered versions of each sub-time series of 100 points. The Savitsky-Golay filter has the advantage of providing smoothing without loss of resolution and of avoiding the distortion of the moments of the signal of all orders up to the order of the polynomial. We vary N_L and M over rather broad intervals to check for the sensitivity of this filtering process and to avoid the occurrence of spurious frequencies that may be created by the filter (see Appendix A).
3. For each of the 24 filtered versions of each sub-time series of 100 points, we use its local polynomial representation to calculate analytically its local derivative by simply differentiation the polynomial associated with each point along the time series. The step constructs an observable which is sensitive to the phase.
4. For each time series of the derivative, we identify the time t_{\max} of the local maximum closest to its middle point. This is analogous to identifying a local maximum of the control parameter of the “canonical” averaging method described above [36, 21].
5. We then translate the origin of time of each derivative time series to this time t_{\max} . This is the “re-phasing” step.
6. For a given N_L and M , we perform the average of the 20 time series derivatives. Varying N_L between 5 and 10 and M between 4 and 7, both by unit increments, provides a total of 24 averaged time series derivatives that are shown in Fig. 4. This is the “canonical” averaging step. The figure is not unlike the local correlation structure $g(r)$ obtained in the probing of the local order of liquids around a representative molecule. In particular, the oscillations decay in amplitude as a function of the distance to the central peak. Note that our choice of rephasing the local maximum closest to its middle point (and not other point) of each time series provides the best choice in order to observe a maximum number of oscillations.

7. For each of the 24 averaged time series derivatives, we perform a Lomb periodogram analysis in order to extract the most probable frequency of each signal. Figure 5 shows the corresponding 24 Lomb spectra. A significant fraction of the 24 Lomb spectra exhibit a very strong and statistically significant thin peak at the correct frequency $f = 1 \pm 0.05$. Other spurious peaks are also present: they result from the interplay between Savitsky-Golay smoothing procedure and the phase noise.
8. To confirm that the information on the existence of the deterministic signal at the frequency $f = 1$ is present in each of the 24 Lomb spectra, Fig. 6 shows the average over these 24 Lomb spectra in Fig. 5. A very clear peak at $f = 1.03 \pm 0.1$ is obtained with an amplitude twice as big as the background.

We have presented here our new method on an extreme case of phase disorder. For smaller disorder, for instance already with $A = 0.1$, the signal obtained with our method is overwhelming while the direct Fourier spectral analysis or even the third method of direct Lomb averaging provide still inconclusive proof of the existence of a deterministic frequency.

We now present the application of this technique for the detection of log-periodicity in the moments of the energy dissipation rate.

3 Detection of log-periodicity in the moments of the energy dissipation rate

3.1 Standard preliminary tests on the experimental data

Very good quality high-Reynolds turbulence data have been collected at the S1 ONERA wind tunnel by the Grenoble group from LEGI [2]. We use the longitudinal velocity data obtained from this group to check for the possible presence of log-periodic undulation in moments of the energy dissipation rate. Figure 7 shows a typical sample of the time series of the streamwise component of the flow velocity, denoted as v hereafter in this work.

The mean velocity of the flow is approximately $\langle v \rangle = 20\text{ms}^{-1}$ (compressive effects are thus negligible). The root-mean-square velocity fluctuations is $v_{\text{rms}} = 1.7\text{ms}^{-1}$, leading to a turbulence intensity equal to $I = v_{\text{rms}}/\langle v \rangle = 0.0826$. This is sufficiently small to allow for the use of Taylor's frozen flow hypothesis. The integral scale is approximately 4m but is difficult to estimate precisely as the turbulent flow is neither isotropic nor homogeneous at these large scales.

The Kolmogorov microscale η is given by [32] $\eta = \left[\frac{\nu^2 \langle v \rangle^2}{15 \langle (\partial v / \partial t)^2 \rangle} \right]^{1/4} = 0.195\text{mm}$, where $\nu = 1.5 \times 10^{-5} \text{m}^2 \text{s}^{-1}$ is the kinematic viscosity of air. $\partial v / \partial t$ is evaluated by its discrete approximation with a time step increment $\partial t = 3.5466 \times 10^{-5} \text{s}$ corresponding to the spatial resolution $\delta_\ell = 0.72\text{mm}$ divided by $\langle v \rangle$.

The Taylor scale is given by [32] $\lambda = \frac{\langle v \rangle v_{\text{rms}}}{\langle (\partial v / \partial t)^2 \rangle^{1/2}} = 16.6\text{mm}$. The Taylor scale is thus about 85 times the Kolmogorov scale. The Taylor-scale Reynolds number is $Re_\lambda = \frac{v_{\text{rms}} \lambda}{\nu} = 2000$. This number is actually not constant along the whole data set and fluctuates by about 20%.

We have analyzed a total number of about $\mathcal{N} = 1.4 \times 10^7$ data points provided in 200 segments of $2^{16} = 65536$ data points. In order to implement our detection method presented in section 2.3, we have re-partitioned the total data set of \mathcal{N} points into N "records" of length L . In the sequel, we present results for $N = 100$ records of length $L = 2^{17} \approx 130,000$ data points ($N \times L = \mathcal{N}$) and for $N = 20$ records of $L = 5 \times 2^{17} \approx 655,000$ data points. Having $N = 100$ (or $N = 20$ respectively)

such records will allow us to test for the reproductivity and stationarity of the results. Each of the N records of length L is then itself subdivided into “samples” of $2^{11} = 2,048$ data points. We thus have 64 (respectively 320) samples per record for $L = 2^{17}$ (respectively for $L = 5 \times 2^{17}$). Taking an integral scale of $\ell_0 = 4\text{m}$ with one point per 0.72mm , a complete turnover covers approximately $2\ell_0/\delta_\ell \approx 10^5$ data points. Each sample thus covers a finite fraction ($\approx 1/5$) of a turn-over time.

We have checked that the turbulent velocity time series recovers the standard scaling laws previously reported in the literature with similar quality. In particular, we have verified the validity of the power-law scaling $E(k) \sim k^{-\beta}$ with an exponent β very close to $\frac{5}{3}$ over a range more than two decades, similar to Fig. 5.4 of [13] provided by Y. Gagne and M. Marchand on a similar data set from the same experimental group. Similarly, we have checked carefully the determination of the inertial range by combining the scaling ranges of several velocity structure functions [14] (see also Fig. 8.6 of [13]). Conservatively, we are led to a well-defined inertial range $60 \leq \ell/\eta \leq 2000$.

3.2 Moments of the energy dissipation rate

Using Taylor’s hypothesis which replaces a spatial variation of the fluid velocity by a temporal variation measured at a fixed location, the rate of kinetic energy dissipation at position i is

$$\epsilon_i \sim [(v_{i+1} - v_i) / \delta_\ell]^2, \quad (5)$$

where δ_ℓ is the resolution (translated in spatial scale) of the measurements. The total dissipation rate E_ℓ in a spatial domain Ω of size ℓ is

$$E_\ell = \delta_\ell \sum_{\Omega_i \in \Omega} \epsilon_i, \quad (6)$$

where Ω_i is the i th sub-piece of linear dimension δ_ℓ in Ω , such that $\Omega_i \cap \Omega_j = \Phi$ for $i \neq j$ and $\bigcup_i \Omega_i = \Omega$. We use normalized energy dissipation E_ℓ/E_L , where L is the size of the system, and normalized scale ℓ/η .

We study the q -th moment of the normalized energy dissipation rate

$$M_q(\ell) = \sum (E_\ell/E_L)^q, \quad (7)$$

as a function of the scale ℓ . The summation in (7) is performed over all domains of size ℓ within the system of size L . The signature of multifractal scaling is that the scaling law

$$M_q(\ell) \sim (\ell/\eta)^{\tau(q)}, \quad (8)$$

is expected to hold in the inertial range with moment exponents $\tau(q)$ that are non-linear functions of q . Using standard arguments [35, 15, 13], the multifractal spectrum $f(\alpha)$ is the Legendre transform of $\tau(q)$. The validity of these power laws (8) and multifractality have been verified with a good accuracy in experiments [32, 13]. We have reproduced these results reliably. As already mentioned, one can discern sometimes some small noisy oscillations, which are suggestive of log-periodicity.

3.3 Canonical averaging of the moment exponents

In order to test for the possible existence of DSI, we apply the methodology explained in section 2.3 to each of the N records of length $L = 2^{17}$. We estimate the moments $M_q(\ell)$ defined by (8) in the range $\ell/\eta \in [216, 1840]$ which is well within the inertial range for each sample. The lower boundary 216 is 3.6 times larger than the lower bound 60 of the inertial range previously discussed, in order to avoid the effect of very small scales that make the signal more noisy.

1. Given a record of length $L = 2^{17}$ (resp. $L = 5 \times 2^{17}$), we cut it into 64 (resp. 320) samples of size 2^{11} points.
2. We then calculate the local moment exponent $\tau(q, \ln(\ell/\eta))$ as the logarithmic derivative of $M_q(\ell)$ with respect to ℓ/η :

$$\tau(q, \ln(\ell/\eta)) = \frac{d \ln(M_q(\ell))}{d \ln(\ell/\eta)}. \quad (9)$$

3. For each sample, we then identify the sample-dependent reduced scale ℓ_c/η closest to the central point of the scale-interval of the analysis at which $\tau(q, \ln(\ell/\eta))$ is maximum.
4. We rephase all functions $\tau(q, \ln(\ell/\eta))$ of the variable $\ln(\ell/\eta)$ of each sample so that their ℓ_c/η coincide. This allows us to define the reduced variable $\Delta \equiv \ln(\ell/\eta) - \ln(\ell_c/\eta)$ such that all functions $\tau(q, \Delta)$ are rephased at $\Delta = 0$.
5. We then average these rephased functions $\tau(q, \Delta)$. This defines the function (local average exponent)

$$D(\Delta) = \langle \tau(q, \Delta) \rangle, \quad (10)$$

where the average is performed over the different samples in one record at fixed $\Delta = \ln(\ell/\eta) - \ln(\ell_c/\eta)$ (where $\ln(\ell_c/\eta)$ vary from sample to sample and $\ln(\ell/\eta)$ is adjusted accordingly).

6. We then perform several comparative analysis to check the quality of the results discussed in the following.

3.4 Results

First, let us stress that our results presented below have been found to yield the same set of log-frequencies, within numerical accuracy, independently of the moment orders varying from $q = 1$ to 19. Appendix B proposes a simple multifractal model explaining this observation. The standard deviation of the log-frequencies discussed below determined from the $N = 100$ records of length $L = 2^{17}$ shows that it is larger for $q = 1$ and reaches a plateau at $q = 3$. We have thus chosen to present the following results for $q = 3$.

Figure 8 shows the canonically averaged local log-derivative $D(\Delta)$ defined in (10) as a function of Δ (left panels) and their corresponding Lomb periodograms (right panels) for three choices of the Savitsky-Golay filter parameters N_L and M . This analysis is performed over the 64 samples of a single record of length $L = 2^{17}$ points.

Rather strong periodic oscillations can be observed on the local average exponent $D(\Delta)$, which results in the high Lomb peaks in the right panels which have good statistical significance [37, 53]. As expected, the central oscillation at $\Delta = 0$ is the largest and the undulations on both side decay as a result of the progressively increasing destructive interference due to noise. One can also note a slight left-right asymmetry that we attribute to the stronger noise affecting the small scales ($\Delta < 0$) compared to the large scales ($\Delta > 0$).

While the undulations and their Lomb spectra seem convincing, there is a problem that seems at first sight to destroy the evidence of a genuine log-periodicity: the periods of the oscillations are strongly dependent upon the parameters N_L and M of the Savitsky-Golay filter (see Appendix A): it would thus seem that we are quantifying spurious oscillations created by the massaging of the data. A similar effect has been found earlier associated with the construction of cumulative

quantities [18]. In order to understand the possible origin of the strong variations in significant log-frequencies as a function of N_L and M and following Ref. [45], we have collected the two most significant log-frequencies (two highest Lomb peaks) of all the 2400 Lomb periodograms available from our analysis of 100 independent records by the 24 possible filters (spanning $N_L = 5 - 10$ and $M = 4 - 7$) used for each record. Fig. 9(a) (respectively (b)) shows the histogram of the log-frequencies associated with the largest (respectively second largest) Lomb peaks. The vertical dashed lines correspond to log-frequencies equal respectively to $f_1 = 1.44$, $f_2 = 2f_1 = 2.89$, $f_3 = 3f_1 = 4.33$, $f_4 = 4f_1 = 5.77$ and $f_5 = 5f_1 = 7.21$. These values correspond respectively to increasing harmonics of a fundamental frequency $f_1 = 1/\ln \gamma$ associated with the scale ratio $\gamma = 2$. Remarkably, similar histograms (but with smaller amplitudes for the peaks at f_2 and f_3) are also obtained by collecting the frequencies corresponding to the third and fourth largest Lomb peaks among the 2400 available Lomb periodograms. The existence of these 5 harmonic frequencies is thus a very robust feature. Another evidence of the quality of the description in terms of 5 harmonics of a fundamental frequency, we represent in Fig. 10 the value of the frequency measured at the n th maximum of the histogram shown in Fig. 9(a) as a function of the order n of the maximum. The straight line shows the excellent linear fit to the equation $f_n = nf_1$, where the sole adjustable parameter f_1 is found equal to $f = 1.62 \pm 0.1$. This value corresponds to a preferred scaling ratio of the cascade equal to $\gamma = 1.85 \pm 0.1$.

We are now in position for explaining the strong variations in the position of the Lomb peaks observed in Fig. 8. Since each filter has a different passing-band (see Appendix A), for a periodic signal which has harmonics of a fundamental frequency with strong amplitudes, these different harmonics will be differently expressed by the different filters. This is what we observe in Fig. 8. The two top panels correspond to the filter with $(N_L = 10, M = 4)$ which selects preferentially the fundamental frequency f_1 . The two middle panels correspond to the filter with $(N_L = 9, M = 5)$ which selects preferentially the second harmonic $f_2 = 2f_1$. Finally, the two bottom panels correspond to the filter with $(N_L = 8, M = 7)$ which selects preferentially the third harmonics $f_3 = 3f_1$. Furthermore, the fact that the second or third harmonics have a larger amplitude than the fundamental frequency is not a surprise and is found for instance in multifractal measures constructed on DSI fractal geometries [54].

The limited bandwidth of each filter and their selection of different harmonics is further quantified by Table 1 which explores the range of values N_L from 5 to 10 and M from 4 to 7, corresponding to a total of 24 filters. Each filter is applied to each of the $N = 100$ records of length $L = 2^{17}$ to obtain the canonically averaged $D(\Delta)$ from which we obtain the corresponding 100 log-frequencies as explained in section 3.3. The average $\langle f \rangle$ of these 100 log-frequencies and their standard deviation σ_f are given as a function of M and N_L in Table 1. $\langle f \rangle$ increases with increasing M and/or decreasing N_L , an expected property of the Savitsky-Golay filter (see Appendix A). This is not however where lies the potentially useful information. To retrieve it, we identify ten pairs (M, N_L) , specifically $(4, 6)$, $(4, 7)$, $(4, 10)$, $(5, 8)$, $(5, 9)$, $(5, 10)$, $(6, 8)$, $(6, 9)$, $(6, 10)$, and $(7, 8)$, whose $\sigma_f \leq 0.3$, i.e., such that there is good confidence in the determination of a log-frequency. Interestingly, these ten pairs give three groups of log-frequencies: (1) eight pairs marked by astroids (*) have an averaged log-frequencies in the range $2.71 - 2.99$; (2) one pair marked by the star (★) has $\langle f \rangle = 4.37$; (3) one pair marked by the circle (○) has $\langle f \rangle = 1.79$. These three frequency bands are in good agreement with the values for the harmonics $f_1 = 1.44$, $f_2 = 2f_1 = 2.89$ and $f_3 = 3f_1 = 4.33$ already discussed.

Note also that there are pairs, say $(M = 5, N_L = 7)$ and $(M = 6, N_L = 7)$, leading to very large standard deviations and values for $\langle f \rangle$ that are far from any of the frequencies $f_1, 2f_1, 3f_1, 4f_1, \dots$. This apparent negative result actually hides a remarkable confirmation of our

| $\langle f \rangle \pm \sigma_f$ | $N_L = 5$ | $N_L = 6$ | $N_L = 7$ | $N_L = 8$ | $N_L = 9$ | $N_L = 10$ |
|----------------------------------|-----------------|-------------------|-------------------|-------------------|-------------------------|-----------------------|
| $M = 4$ | 3.63 ± 0.91 | $2.89 \pm 0.20^*$ | $2.71 \pm 0.27^*$ | 2.51 ± 0.49 | 2.18 ± 0.81 | $1.79 \pm 0.20^\circ$ |
| $M = 5$ | 5.22 ± 0.63 | 4.32 ± 0.36 | 3.76 ± 0.70 | $2.99 \pm 0.25^*$ | $2.85 \text{ pm}0.14^*$ | $2.76 \pm 0.16^*$ |
| $M = 6$ | 5.22 ± 0.64 | 4.31 ± 0.36 | 3.78 ± 0.69 | $3.01 \pm 0.28^*$ | $2.85 \text{ pm}0.14^*$ | $2.77 \pm 0.11^*$ |
| $M = 7$ | 6.15 ± 0.66 | 5.72 ± 0.63 | 4.82 ± 0.55 | $4.37 \pm 0.27^*$ | $3...90 \pm 0.60$ | 3.13 ± 0.43 |

Table 1: Averaged logarithmic frequencies $\langle f \rangle$ as a function of M from 4 to 7 and N_L from 5 to 10 of the Savitsky-Golay filter. We use $6 \times 4 = 24$ versions of the Savitsky-Golay filter to test for the sensitivity of the order M of the fitting polynomial and the number $2N_L + 1$ of points. This 24 filters allow us to sweep broadly a large range of possible log-frequencies and thus to access the fundamental log-frequency f_1 and several of its harmonics.

| $\sigma_f / \langle f \rangle$ | $N_L = 5$ | $N_L = 6$ | $N_L = 7$ | $N_L = 8$ | $N_L = 9$ | $N_L = 10$ |
|--------------------------------|-----------|-----------|-----------|-----------|-----------|------------|
| $M = 4$ | 0.25 | 0.07* | 0.10* | 0.20 | 0.37 | 0.11 |
| $M = 5$ | 0.12 | 0.08* | 0.19 | 0.08* | 0.05* | 0.06* |
| $M = 6$ | 0.12 | 0.08* | 0.18 | 0.09* | 0.05* | 0.04* |
| $M = 7$ | 0.11 | 0.11 | 0.11 | 0.06* | 0.15 | 0.14 |

Table 2: Relative deviations $\sigma_f / \langle f \rangle$ of the averaged log-frequencies already shown in Table 1 as a function of the parameters M and N_L of the Savitsky-Golay filter.

previous presentation. Indeed, Fig. 11(a) shows the detected log-frequencies f of the 100 different records calculated for different orders q of the moments of the energy dissipation rate for ($M = 5, N_L = 10$). Note first that the determined frequency for $q = 1$ fluctuates more than for higher moment orders $q > 1$, which justifies our investigation of different moment orders. Secondly, the arrow shows a large fluctuation occurring for record 74: while most of the records are tuned to the frequency $f_2 = 2f_1$, record 74 selects f_1 as its best log-frequency. This provides a mechanism in which the competition between the different first frequencies can lead to an average in between as found in Table 1 for ($M = 5, N_L = 7$) and ($M = 6, N_L = 7$). Figure 11(b) shows all the Lomb periodograms obtained for record 74: we directly visualize in this case the strong competition between the two first log-frequencies f_1 and f_2 , strengthening the case for the existence of a discrete set of log-frequencies.

Table 2 offers another perspective to this analysis by showing the relative deviations $\sigma_f / \langle f \rangle$ of the average log-frequencies shown in Table 2. To illustrate the robustness of the recovery of the main harmonics of the fundamental frequency f_1 , let us select only those log-frequencies determined with a relative precision better than 0.10. We find now two classes of pairs (M, N_L) of filters. The first class contains (4, 6), (4, 7), (5, 8), (5, 9), (5, 10), (6, 8), (6, 9) and (6, 10) and is marked by the astroid (*) and corresponds to $\langle f \rangle \simeq 2.71 - 2.99$. The second class contains (2) (5, 6), (6, 6) and (7, 8) and is marked by the stars (*) and corresponds to $\langle f \rangle \simeq 4.31 - 4.37$.

Increasing the size L of the records improves the quality of the signal. This is first quantified by Figs. 12-15 in which the dashed lines corresponding to $L = 5 \times 2^{17}$ give larger and thinner peaks than the continuous lines obtained for $L = 2^{17}$ (see below). This confirms the role of our canonical averaging procedure which improves in quality as the number of samples used in the averaging

| $\langle f \rangle (\sigma_f / \langle f \rangle)$ | $N_L = 5$ | $N_L = 6$ | $N_L = 7$ | $N_L = 8$ | $N_L = 9$ | $N_L = 10$ |
|--|------------|------------|------------|------------|------------|------------|
| $M = 4$ | 3.68(0.20) | 2.90(0.03) | 2.82(0.04) | 2.67(0.08) | 1.92(0.18) | 1.78(0.05) |
| $M = 5$ | 5.38(0.11) | 4.38(0.02) | 4.07(0.12) | 2.96(0.03) | 2.84(0.02) | 2.82(0.02) |
| $M = 6$ | 5.53(0.08) | 4.38(0.06) | 4.06(0.12) | 2.96(0.04) | 2.84(0.03) | 2.80(0.02) |
| $M = 7$ | 6.34(0.11) | 5.74(0.02) | 4.72(0.10) | 4.40(0.02) | 4.33(0.02) | 2.90(0.04) |

Table 3: Log-frequencies $\langle f \rangle$ and relative deviations $\sigma_f / \langle f \rangle$ as a function of M and N_L for the records of length $L = 5 \times 2^{17}$.

increases. Table 3 gives the log-frequencies $\langle f \rangle$ and their corresponding relative deviations $\sigma_f / \langle f \rangle$ as a function of M and N_L of the Savitsky-Golay filter for the $N = 20$ records of length $L = 5 \times 2^{17}$. Comparing Table 3 ($L = 5 \times 2^{17}$) with Tables 1 and 2 ($L = 2^{17}$), we find that a larger L leads to a clearer determination of the harmonics log-frequencies. For instance, keeping all frequencies such that the relative error $\sigma_f / \langle f \rangle$ is less than 0.1, we find that all the determined log-frequencies now very close the exact values of the harmonics of $f_c = 1.44$. This confirms an important expectation of our canonical averaging procedure: using more samples will definitely improve its efficiency for extracting some hidden fundamental log-frequency and/or its harmonics.

Figures 12-15 summarize our analysis by presenting the Lomb periodogram obtained by averaging over the $N = 100$ (respectively $N = 20$) records of length $L = 2^{17}$ (respectively $L = 5 \times 2^{17}$), for each of the 24 Savitsky-Golay filters described above. All the five harmonics of the fundamental frequency f_1 discussed above are seen to correspond to the main peaks of the Lomb periodograms with a good approximation. It is expected that their amplitude should vary with the filter, in response to the frequency selection of each filter. It is quite remarkable however to obtain such a strong coherence of the peaks over all the filters. This coherence is further demonstrated by taking the average over all $24 \times N$ Lomb periodograms (24 filters for each of the N records) which is shown in Fig. 16. Notice the good agreement between the values of the log-frequencies corresponding to the peaks and the prediction from DSI with a root scaling ratio $\gamma = 2$ (shown as the dashed vertical lines). We attribute the only significant deviation observed for the first harmonics f_1 to a combination of two factors: (1) the amplitude of the Lomb peak is small and its maximum is thus mechanically biased by the existence of the second large peak at f_2 ; (2) as we have seen, different filters have different bandwidth and the averaging of a relatively low signal will lead to unavoidable distortions.

3.5 Statistical significance

The statistical significance of a Lomb peak requires in principle the specification of the properties (distribution function and dependence) of the noise decorating the signal. The simplest and most often used noise is the Gaussian white noise for which the statistical significance level of the highest Lomb peak can be determined analytically [42, 16, 37]. It gives an approximately exponentially decaying false-alarm probability:

$$Pr(> z) = 1 - (1 - e^{-z})^{M'} \sim M' e^{-z}, \quad (11)$$

where M' is proportional to the number of data points.

In practice, noise is almost never Gaussian white noise with often much fatter tails of the distribution and possible short or long-range correlations. Extensive numerical simulations have in-

investigated the impact of heavy-tailness, of correlations and of the interplay between them on the significance level of a Lomb periodogram peak [53]. It was found that the worst case leading to high false-alarm probabilities correspond to a persistent fractional Brownian noise with large Hurst exponent. Consider for instance the highest Lomb peak with height 16.5 presented in Fig. 14(f) as the dashed line, obtained with 52 data points. According to the simulations of Ref. [53], this can be translated into a false-alarm probability of 0.1% and a statistical confidence of 99.9%, even for the worst case of a strongly persistent fractional Gaussian noise with Hurst exponent $H = 0.9$. For a Lomb peak of height 10 as shown in Fig. 14(b) as the dashed lines, the confidence level is about 99.95% for a fractional Brownian noise with $H = 0.7$ and ~ 0.99 with $H = 0.8$.

We have performed additional simulations to test whether the five log-frequency harmonics obtained from the Lomb peaks in Figs. 12-15 of the turbulent data could result from the strongest case of spurious log-periodicity [53, 18], namely when the noise exhibits a strong persistence with long-range correlations. We would like to compare the probability for obtaining a large Lomb peak in a purely synthetic fractional Brownian noise with a large Hurst exponent, using exactly the canonical averaging procedure used for analyzing the turbulence data. It is known [53, 18] that, the larger H is, the stronger are the spurious log-periodic undulations. Specifically, we use fractional Gaussian noises of Hurst exponent $H = 0.99$ to replace the original fluctuations decorating the leading power law of the moments for each sample and follow exactly the same analysis procedure as for the turbulence data. We generated 100 data sets of fractional Gaussian noises with the Hurst exponent $H = 0.99$, each set having 61 data points. The Lomb periodograms averaged over 100 samples, corresponding to different M and N_L of the Savitsky-Golay filter, are shown in Fig. 17. Compared with Figs. 12-15, the main feature of the Lomb periodograms in Fig. 17 is that there are no harmonics visible and the extracted frequencies appear completely random. This is in strong contrast with the analysis for the turbulence data which exalts the five log-periodic frequency harmonics. Moreover, the histogram of the total 2400 log-frequencies corresponding to the highest peaks of the 24×100 Lomb periodograms, shown in Fig. 18, does not indicate that any frequency is playing a special role. The same qualitative results are found when varying the Hurst exponent H between 0.5 to 0.99.

In summary, while the Savitsky-Golay filter leads to strong spurious log-periodic components in the fractional Gaussian noises with high Hurst exponent, their large dispersion from one filter to the other rules out that such a noise can be at the origin of the log-periodicity uncovered from our analysis. In addition, since the fractional Gaussian noises with high Hurst exponents are by far the processes leading to the largest spurious log-periodicity, this test also excludes all reasonable types of noise investigated previously [53, 18], such as for GARCH(1,1) noise with Student distributions with different numbers of degrees of freedom, for power law noises, for Lévy stable noise as well as of course for independent Gaussian noise.

4 Conclusions

We have presented the results of a search for the existence of log-periodic oscillations decorating the moments of the energy dissipation rate in experimental data at high Reynolds number (≈ 2500) of three-dimensional fully developed turbulence. We have proposed a simple dynamical representation of the Richardson-Kolmogorov cartoon of a cascade that explains why standard averaging techniques erase by their construction the possible existence of log-periodic corrections to scaling associated with a discrete hierarchy. We have introduced a novel “canonical” averaging methodology for extracting a possible log-periodic signal in turbulence time series and have tested it on

synthetic examples constructed to capture the interplay between a weak log-periodic component and rather strong multiplicative and phase noises. The many tests presented confirm the remarkable observation of statistically significant log-periodic correction to scaling, with a preferred scaling ratio for length scales compatible with the value $\gamma = 2$. A strong confirmation of this result is provided by the identification of up to 5 harmonics of the fundamental log-periodic undulations, associated with up to 5 levels of the underlying hierarchical dynamical structure.

Acknowledgments: The experimental turbulence data obtained at ONERA Modane were kindly provided by Y. Gagne. We are grateful to J. Delour and J.-F. Muzy for help in pre-processing these data. This work was partially supported by NSF-DMR99-71475 and the James S. Mc Donnell Foundation 21st century scientist award/studying complex system.

| $\langle f \rangle / f_c$ | $N_L = 5$ | $N_L = 6$ | $N_L = 7$ | $N_L = 8$ | $N_L = 9$ | $N_L = 10$ |
|---------------------------|-----------|-----------|-----------|-----------|-----------|------------|
| $M = 4$ | 1.87 | 1.82 | 0.81 | 1.02 | 1.00 | 1.04 |
| $M = 5$ | 3.04 | 1.87 | 2.04 | 1.82 | 1.07 | 0.98 |
| $M = 6$ | 3.04 | 2.04 | 2.00 | 2.00 | 1.87 | 1.42 |
| $M = 7$ | 3.11 | 3.02 | 1.99 | 1.95 | 2.04 | 1.99 |

Table 4: Ratios of the frequencies (divided by f_c) extracted from the largest peak of the average of 10 Lomb periodograms of a synthetic signal with 4 harmonics and a large centered Gaussian white noise with standard deviation $\sigma_e = 3$ as a function of the two parameters M and N_L of the Savitsky-Golay filter.

Appendix A: Study of the bandwidth selectivity of the Savitsky-Golay filter

By construction, the Savitsky-Golay filter has a finite bandwidth, i.e., it not only filters out high frequencies but also enhances preferentially an intermediate frequency band whose determination depends on its two parameters, the order M of the fitting polynomial and the number $2N_L + 1$ over which this fit is performed. Let us make this remark quantitative.

Consider a periodic function with four harmonics of the fundamental frequency f_c

$$y(t) = \cos(2\pi f_c t) + \cos(4\pi f_c t) + \cos(6\pi f_c t) + \cos(8\pi f_c t) + e, \quad (12)$$

where $f_c = 1/\ln 2$, t is evenly spaced in $[-1, 1]$ with 61 points and the noise e is normally distributed with zero mean and standard deviation $\sigma_e = 3$. This choice is reasonably close to the situation found the turbulence data, in that several harmonics and noise compete with similar amplitudes.

We generate 10 times series of 61 points with t regularly spaced in $\in [-1, 1]$. For each of these times series, we choose one pair (M, N_L) and apply the Savitsky-Golay filter. We then apply the Lomb periodogram technique on the resulting smoothed time series to obtain a Lomb spectrum. We average the 10 Lomb spectra and identify the frequency of the largest peak which is reported in the Table 4. Actually, we show the ratios of the extracted frequencies to f_c . Remarkably, 17 frequencies among the 24 (i.e., 71%) are found to within less than 10% from one of the harmonics $f_c, 2f_c, 3f_c$. The 7 remaining frequencies are within less than 20% from one of the harmonics $f_c, 2f_c, 3f_c$. The second observation is that, indeed, a given filter (M, N_L) amplifies selectively on average one harmonics at the expense of the other. Interestingly, when increasing the noise amplitude σ_e , the fourth harmonic $4f_c$ is also sampled by a few filters. Obviously, when the amplitude of the noise is very large, spurious frequencies are selected but come with a low statistical significance. With large noise and some combinations of the amplitudes of the harmonics in (12), the artifactual frequency $f_m = 1.5/\ln 2$ appears; its origin has been unravelled in Ref. [18, 19] as corresponding to the most probable noise structure. For very large noise, we can also identify a kind of effective non-linear coupling between the frequencies leading to combinations of the harmonics [6].

We have performed many tests with pure noise, with a single cosine plus noise and with several harmonics plus noise. In the first case, the frequencies obtained as the maxima of the Lomb spectra do not exhibit any preferred value and fluctuate broadly from realization to realization. With a single oscillatory signal, we see a clear peak in the Lomb spectrum, broadened by the disorder. In the case of several harmonics of a fundamental frequency, we find that one of the harmonics in general

dominates each Savitsky-Golay filter, allowing us to detect all the relevant harmonics by using many different filters.

Appendix B: A simple multifractal model with discrete scale invariance (DSI) independent of the moment order q

Our analysis of the log-periodic undulations decorating the power law of the moments of the dissipation rate suggests that the log-frequency of these undulations is independent of the order of the moments used in the analysis. Here, we propose a simple multifractal model with DSI which exhibits this property.

Consider a simple cascade process of the type introduced by the Russian school and studied by Mandelbrot (see [12] and references therein), with however one simple modification emphasizing DSI. Each large eddy \mathcal{F} of size r is assumed to transfer the fraction m_i of its energy to n small eddies \mathcal{F}_i of size $r_i = r/\gamma_i$, $i = 1, 2, \dots, n$, where the pair (m_i, γ_i) each are one of n different fixed values $(m_1, \gamma_1), (m_2, \gamma_2), \dots, (m_n, \gamma_n)$ respectively. Each small eddy of size r_i in turn transfers a fraction m_j to each of its n daughters of size r_i/γ_j , where m_j and γ_j are drawn from the same fixed set $(m_1, \gamma_1), (m_2, \gamma_2), \dots, (m_n, \gamma_n)$. This deterministic multiplicative cascade process continues down to the dissipation scale and creates a self-similar multifractal measure with multipliers and characteristic scaling ratios m_i and γ_i , respectively. We do not restrict the model to obey the space-filling condition $\sum_{i=1}^n 1/\gamma_i = 1$ [12].

Using the self-similarity of the cascade process, we can write

$$M_q(\mathcal{F}; \ell) = \sum_{i=1}^n M_q(\mathcal{F}_i; \ell), \quad (13)$$

where $M_q(\mathcal{F}; \ell)$ is the q th-order moment of the energy dissipation rate defined on eddy \mathcal{F} . According to the self-similarity of the multinomial measure, we have

$$M_q(\mathcal{F}; \ell) = m_i^q M_q(\mathcal{F}_i; \gamma_i \ell). \quad (14)$$

Combining Eqs. (13) and (14) and removing the reference to a specific eddy \mathcal{F} gives the following discrete scale invariant equation [54]

$$M_q(\ell) = \sum_{i=1}^n M_q(\gamma_i \ell) m_i^q. \quad (15)$$

For statistically self-similar measures, Eq. (15) is modified by inserting in each term at the r.h.s. of equation (15) the specific probabilities of the realizations among the n scenarios at each step of the cascade,

Equation (15) generalizes the equation $M_q(\ell) = m^q M_q(\gamma \ell)$ embodying the discrete scale invariance of simple fractals constructed using the iteration of a deterministic rule such as the triadic Cantor set or the Sierpinsky gasket. This equation is discussed in Ref. [30] in relation with so-called “fractal strings”. Looking for a scaling solution $M_q(\ell) \propto \ell^{\tau(q)}$, the exponents $\tau(q)$ are the solutions of

$$\sum_{i=1}^n \gamma_i^{\tau(q)} m_i^q = 1 \quad (16)$$

and form an infinite countable set of complex numbers. For the “lattice” case where there is a common root γ and there are integers k_i such that

$$\gamma_i = \gamma^{k_i}, \quad (17)$$

the solution of (15) can be explicated analytically.

Substituting Eq. (17) into Eq. (15), we have

$$M_q(\ell) = \sum_{i=1}^n M_q(\gamma^{k_i} \ell) m_i^q, \quad (18)$$

whose solution is

$$M_q(\ell) = C(\ell) \ell^{\tau(q)}, \quad (19)$$

where $C(\ell)$ is a universal function and the case of $C(\ell) = \text{const.}$ recovers the familiar power law given in Eq. (8). It is easy to verify that if $C(\ell)$ is a periodic function of the variable $\ln(\ell)$ with the log-period $\ln(\gamma)$, i.e.,

$$C(\ell) = C(\gamma^{k_i} \ell), \quad (20)$$

then Eq. (19) is the solution of Eq. (15). Without loss of generality, we can rewrite the general solution as

$$M_q(\ell) = \psi_q [\ln(\ell) / \ln(\gamma)] \ell^{\tau(q)}. \quad (21)$$

This implies that $M_q(\ell)$ is log-periodic. We emphasize that ψ_q is q -dependent, while the log-period $\ln(\gamma)$ of $M_q(\ell)$ is independent of q . Another important implication is that, given a unique preferred scaling ratio $\gamma = \exp(1/f)$, it is possible to have a set of characteristic scaling ratios γ_i satisfying the lattice condition expressed by Eq. (17) which describe an infinite recursion of the multifractal measure.

References

- [1] Anifrani, J.-C., Le Floc'h, C., Sornette, D. and Souillard, B. (1995) *J.Phys.I France* **5**, pp. 631–638.
- [2] Anselmet, F., Y. Gagne, E.J. Hopfinger and R.A. Antonia, High-order velocity structure functions in turbulent shear flows, *J. Fluid Mech.* 140, 63-89 (1984).
- [3] Arnéodo, A., Argoul, F., Bacry, E., Elezgaray, J. & Muzy, J.-F. *Ondelettes, multifractales et turbulences*, Diderot Editeur, Arts et Sciences (1995).
- [4] Barenblatt, G.I. and Goldenfeld, N., Does fully developed turbulence exist? Reynolds number independence versus asymptotic covariance, *Phys. Fluids* 7, 3078-3082 (1995).
- [5] Benzi, R., S. Ciliberto, R. Tripiccion, C. Baudet, C. Massaioli and S. Succi, Extended self-similarity in turbulent flows, *Phys. Rev. E* 48, R29-R32 (1993).
- [6] Berge, P., Y. Pomeau and C. Vidal, *Order Within Chaos: Towards a Deterministic Approach to Turbulence* (Hermann, Paris, 1984).
- [7] Binder K. and D.W. Heermann, Spin glasses: Experimental facts, theoretical concepts, and open questions, *Rev. Mod. Phys.* 58, 801-972 (1986). (see pp. 838)
- [8] Bonn, D., Y. Couder, P.H.J. van Dam and S. Douady, From small scales to large scales in three-dimensional turbulence: the effect of diluted polymers, *Phys. Rev. E* 47, R28-R31 (1993).
- [9] Castaing, B. (1997) in *Scale invariance and beyond*, eds. Dubrulle, B., Graner, F. & Sornette, D., EDP Sciences and Springer, pp. 225–234.
- [10] Dubrulle, B., Anomalous scaling and generic structure function in turbulence, *J. Phys. France* II 6, 1825-1840 (1996).
- [11] Feigenbaum, J.A., A statistical analysis of log-periodic precursors to financial crashes, *Quantitative Finance* 1 (3), 346-360 (2001)
- [12] Frisch U, Sulem P L, Nelkin M. A simple dynamical model of intermittent fully developed turbulence. *Journal of Fluid Mechanics* 87, 719-736 (1978).
- [13] Frisch U, *Turbulence: The Legacy of A.N. Kolmogorov* (Cambridge University, Cambridge, 1996).
- [14] Gagne, Y. Etude expérimentale de l'intermittence et des singularités dans le plan complexe en turbulence développée, PhD thesis. University of Grenoble (1987).
- [15] Halsey T.C., M.H. Jensen, L.P. Kadanoff, I. Procaccia and B.I. Shraiman, Fractal measures and their singularities: the characterization of strange sets, *Phys. Rev. A* 33, 1141-1151(1986).
- [16] Horne, J.H. and S.L. Baliunas, A Prescription for period analysis of unevenly sampled time series, *Astrophysical Journal* 302, 757-763 (1986).
- [17] Huang Y., G. Ouillon, H. Saleur and D. Sornette, Spontaneous generation of discrete scale invariance in growth models, *Physical Review E* 55, 6433-6447 (1997).

- [18] Huang, Y., A. Johansen, M.W. Lee, H. Saleur and D. Sornette, Artfactual Log-Periodicity in Finite-Size Data: Relevance for Earthquake Aftershocks, *J. Geophys. Res.* 105, 25451-25471 (2000).
- [19] Huang, Y., H. Saleur and D. Sornette, Reexamination of log-periodicity observed in the seismic precursors of the 1989 Loma Prieta earthquake, *J. Geophysical Research* 105, B12, 28111-28123 (2000).
- [20] Johansen, A., D. Sornette, H. Wakita, U. Tsunogai, W.I. Newman and H. Saleur, Discrete scaling in earthquake precursory phenomena : evidence in the Kobe earthquake, Japan, *J.Phys.I France* 6, 1391-1402 (1996).
- [21] Johansen, A. and D. Sornette, Evidence of discrete scale invariance by canonical averaging, *Int. J. Mod. Phys. C* 9, 433-447 (1998).
- [22] Johansen, A., D. Sornette and O. Ledoit, Predicting Financial Crashes using discrete scale invariance, *Journal of Risk* 1 (4), 5-32 (1999).
- [23] Johansen, A. and D. Sornette, Critical ruptures, *Eur. Phys. J. B* 18, 163-181 (2000).
- [24] Johansen, A. and D. Sornette, The Nasdaq crash of April 2000: Yet another example of log-periodicity in a speculative bubble ending in a crash, *European Physical Journal B* 17, 319-328 (2000).
- [25] Johansen, A., H. Saleur and D. Sornette, New Evidence of Earthquake Precursory Phenomena in the 17 Jan. 1995 Kobe Earthquake, Japan, *Eur. Phys. J. B* 15, 551-555 (2000).
- [26] Johansen, A., D. Sornette and A.E. Hansen , Punctuated vortex coalescence and discrete scale invariance in two-dimensional turbulence. *Physica D*, 2000, 138: 302-315.
- [27] Kolmogorov, A.N., A refinement of previous hypotheses concerning the local structure of turbulence in a viscous incompressible fluid at high Reynolds number, *J. Fluid. Dyn.* 13, 82-85 (1962).
- [28] Kraichnan, R.H., A theory of turbulence dynamics, in second symposium on naval hydrodynamics, 29-44, Office of Naval Research, Washington, DC (Ref. ACR-38, 1958).
- [29] Kraichnan, R.H., The structure of isotropic turbulence at very high Reynolds numbers, *J. Fluid. Mech.* 5, 497-543 (1959).
- [30] Lapidus M.L. and M. van Frankenhuisen, *Fractal Geometry and Number Theory: Complex Dimensions of Fractal Strings and Zeros of Zeta Function* (Birkhäuser, Boston, 2000).
- [31] L'vov, V.S., Podivilov, E., Pomyalov, A., Procaccia, I. and Vandembroucq, D., Improved shell model of turbulence, *Phys. Rev. E* 58, 1811-1822 (1998).
- [32] Meneveau C. and K.R. Sreenivasan, The multifractal nature of turbulent energy dissipation, *Journal of Fluid Mechanics* 224, 429-484 (1991).
- [33] Novikov, E.A. (1966) *Dokl. Akad. Nauk SSSR* **168/6**, pp. 1279.
- [34] Novikov, E.A., (1990) *Phys. Fluids A* **2**, pp. 814–820.

- [35] Parisi, G. and U. Frisch, On the singularity structure of fully developed turbulence, in Turbulence and predictability in geophysical fluid dynamics, Proceed. Intern. School of Physics E. Fermi, 1983, Varenna, Italy, 84-87, eds. M. Ghil, R. Benzi and G. Parisi, North Holland, Amsterdam (1985).
- [36] Pázmándi F., R.T. Scalettar and G. T. Zimányi, Revisiting the Theory of Finite Size Scaling in Disordered Systems: ν Can Be Less than $2/d$, Phys. Rev. Lett. 79, 5130 (1997).
- [37] Press, W., S. Teukolsky, W. Vetterling and B. Flannery, Numerical Recipes in FORTRAN: The Art of Scientific Computing (Cambridge University, Cambridge, 1996).
- [38] Renner, C., J. Peinke, R. Friedrich, O. Chanal and B. Chabaud, On the universality of small scale turbulence, preprint physics/0109052.
- [39] Richardson L.F., Weather Prediction by Numerical Process (Cambridge University Press, 1922).
- [40] Saleur, H., C.G. Sammis and D. Sornette, Discrete scale invariance, complex fractal dimensions and log-periodic corrections in earthquakes, Journal of Geophysical Research-Solid Earth 101, 17661-17677 (1996).
- [41] Saleur, H. and D. Sornette, Complex exponents and log-periodic corrections in frustrated systems, J.Phys.I France 6, n3, 327-355 (1996)
- [42] Scargle, J.D., Study in astronomical time series analysis. II. Statistical aspects of spectral analysis of unevenly spaced data, Astrophysical Journal 263, 835-853 (1982).
- [43] Smith L.A., J.D. Fournier and E.A. Spiegel, Lacunarity and intermittency in fluid turbulence, Phys. Lett. A 114, 465-468 (1986).
- [44] Sornette, D. and C.G. Sammis, Complex critical exponents from renormalization group theory of earthquakes : Implications for earthquake predictions, J.Phys.I France 5, 607-619 (1995)
- [45] Sornette, D., A. Johansen, A. Arneodo, J.-F. Muzy and H. Saleur, Complex fractal dimensions describe the internal hierarchical structure of DLA, Phys. Rev. Lett. 76, 251-254 (1996).
- [46] Sornette, D., A. Johansen and J.-P. Bouchaud, Stock market crashes, Precursors and Replicas, J.Phys.I France 6, 167-175 (1996).
- [47] Sornette, D., Discrete scale invariance and complex dimensions, Phys. Rep. 297, 239-270 (1998) (see <http://xxx.lanl.gov/abs/cond-mat/9707012> for an update to 1999).
- [48] Sornette, D., Discrete scale invariance in turbulence? U. Frisch (ed.), Advances in Turbulence VII, 251-254 (Kluwer Academic Publishers, The Netherlands, 1998).
- [49] Sornette, D. and A. Johansen, Significance of log-periodic precursors to financial crashes, Quantitative Finance 1 (4), 452-471 (2001)
- [50] Stauffer, D. and D. Sornette, Log-periodic Oscillations for Biased Diffusion on 3D Random Lattice, Physica A 252, 271-277 (1998)
- [51] Tch  ou, J.-M. & Brachet, M.E. (1996) *J.Phys.II France* **6**, pp. 937-943.

- [52] Wiseman S. and E. Domany, Self-averaging, distribution of pseudocritical temperatures, and finite size scaling in critical disordered systems, *Phys. Rev. E* 58, 2938-2951 (1998).
- [53] Zhou W.-X. and D. Sornette, Statistical Significance of periodicity and log-periodicity with heavy-tailed correlated Noise, Preprint (2001).
- [54] Zhou W.-X. and D. Sornette, Discrete scale invariance in fractals and multifractal measures, 2001, in preparation.

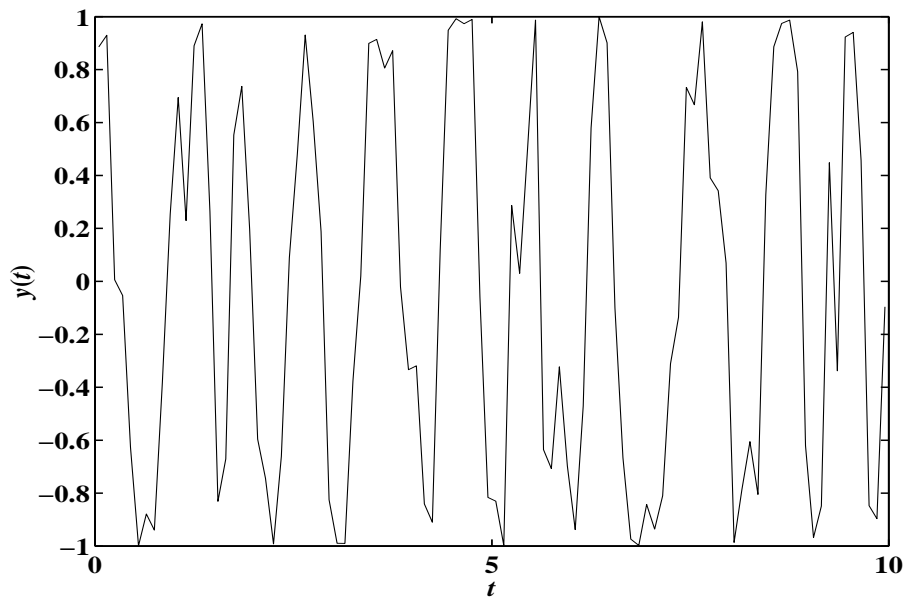


Figure 1: One realization with 100 points of the time series (3,4) with $f = 1, A = 0.3$ generated numerically with $dt = 0.1$ in the time interval $[0, 10]$.

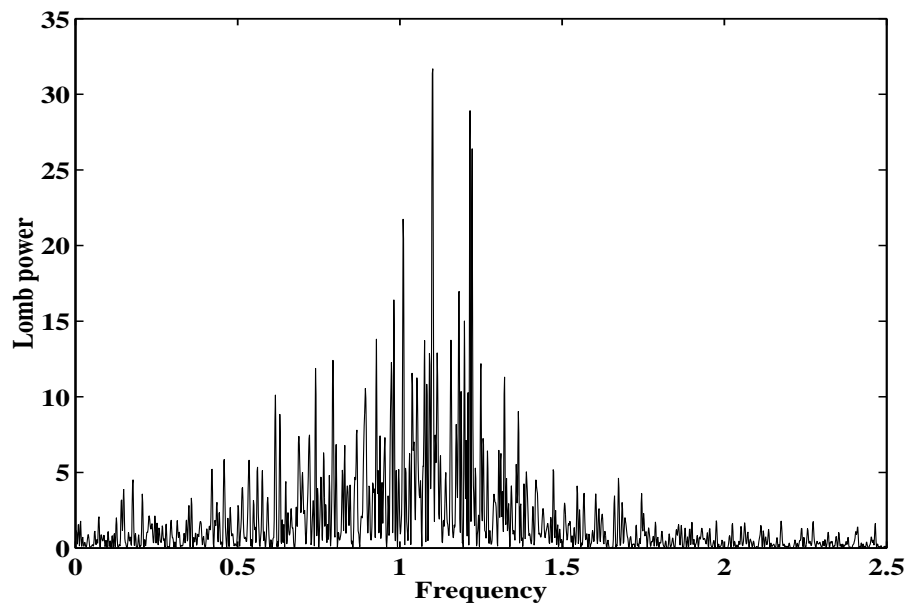


Figure 2: Standard spectral analysis (Fourier spectrum) of a long time series (3,4) with $f = 1$, $A = 0.3$ generated numerically with $dt = 0.1$ in the time interval $[0, 200]$ with 2000 points.

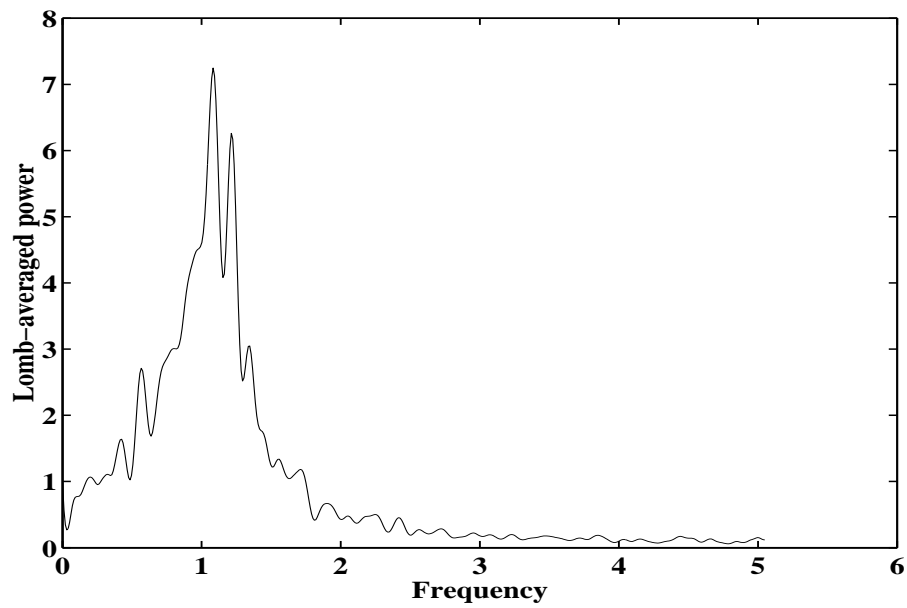


Figure 3: Result of the third method listed in section 2.2 applied to the time series of 2000 points generating to obtain the spectrum shown in Fig. 2. We divide the long time series with 2000 points in 20 contiguous time series of 100 points each that are similar to that represented in Fig. 1. We perform on each of these 20 time series a Lomb periodogram analysis and then average these 20 Lomb periodograms.

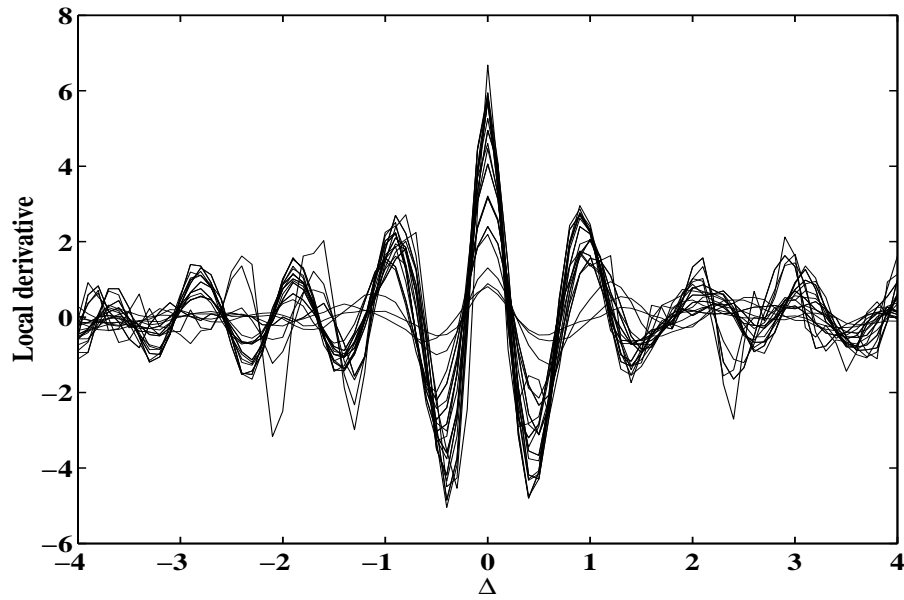


Figure 4: For a given N_L and M , we perform the average of the 20 time series derivatives described in the text. Varying N_L between 5 and 10 and M between 4 and 7, both by unit increments, provides a total of 24 averaged time series derivatives that are shown here.

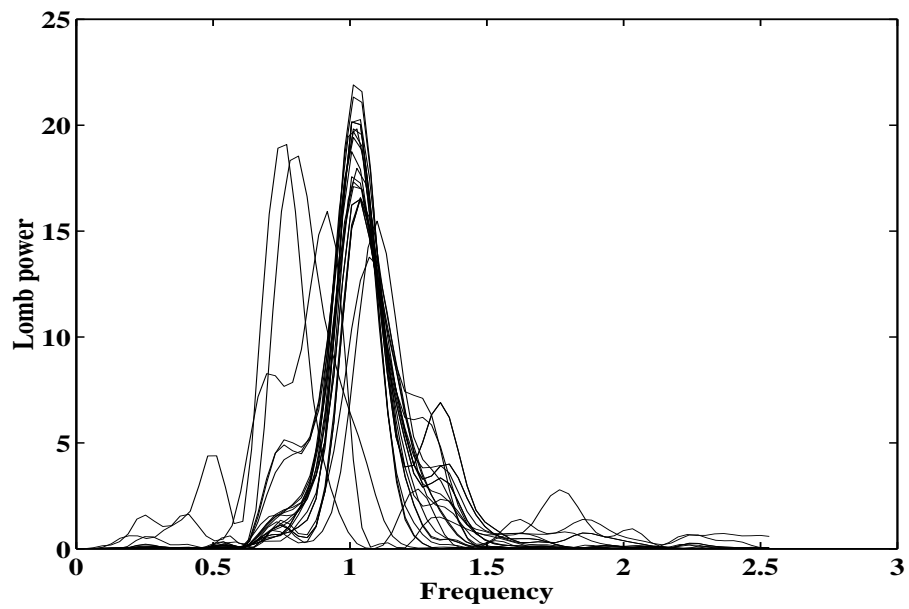


Figure 5: For each of the 24 averaged time series derivatives represented in Fig. 4, we show the corresponding Lomb periodogram spectrum.

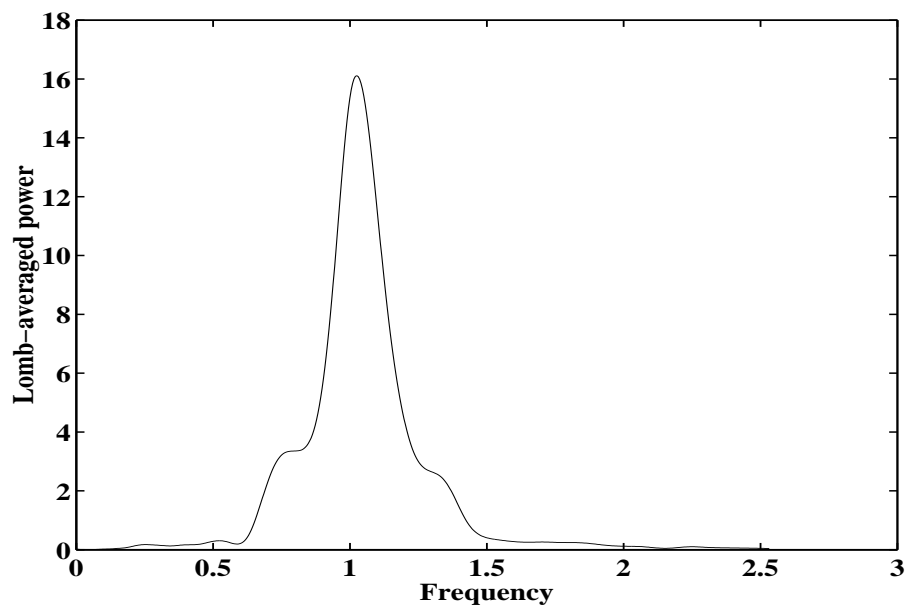


Figure 6: Average over the 24 Lomb spectra shown in Fig. 5.

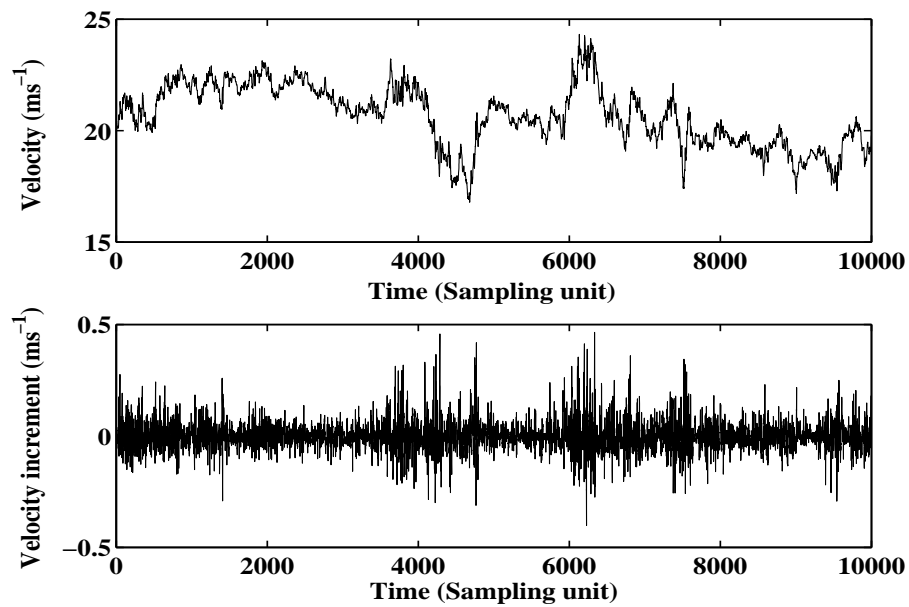


Figure 7: (a) A typical streamwise velocity time series recorded by hot-wire anemometry in the S1 ONERA wind tunnel. (b) Corresponding time series of the velocity increments.

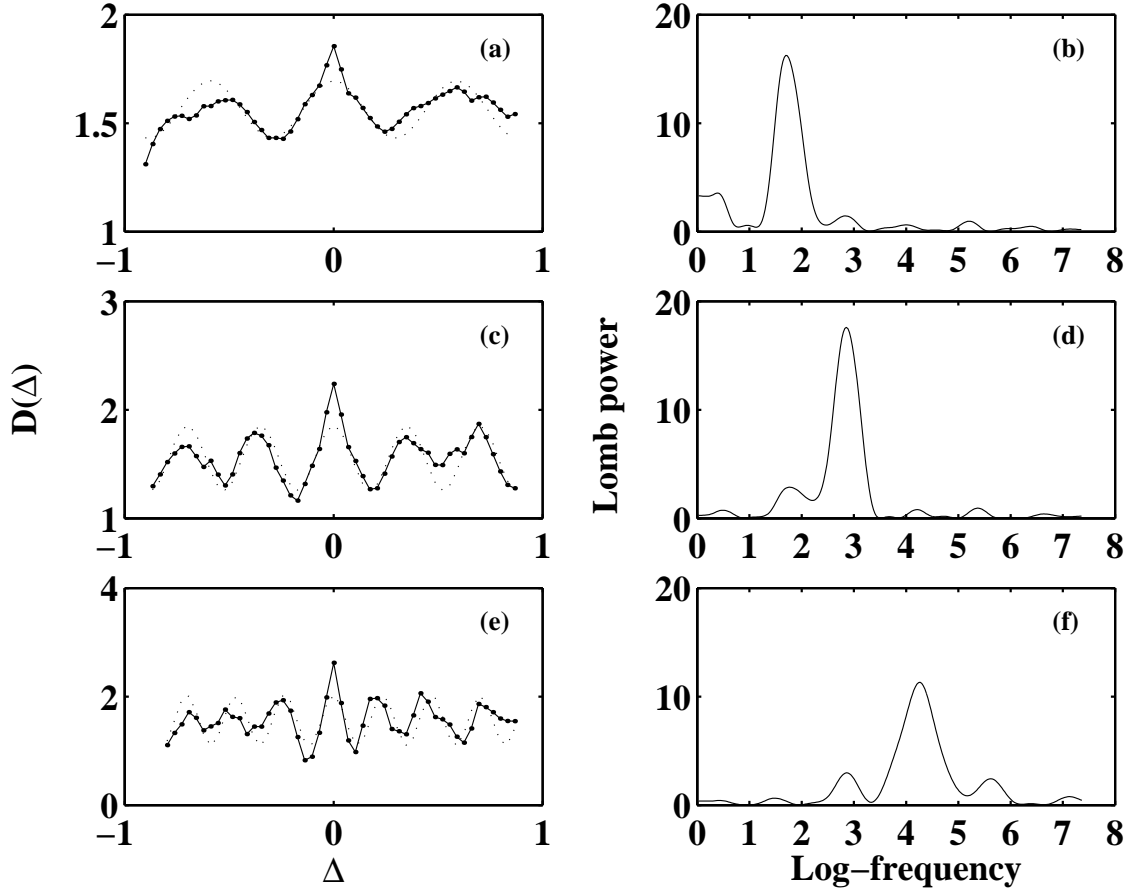


Figure 8: Local log-derivative $D(\Delta)$ defined in (10), canonically averaged over the 64 samples of a single record of length $L = 2^{17}$ points, as a function of Δ (left panels) and their corresponding Lomb periodograms (right panels) for three choices of the Savitsky-Golay filter parameters N_L and M . (a-b) $M = 4$ and $N_L = 10$, (c-d) $M = 5$ and $N_L = 9$, (e-f) $M = 7$ and $N_L = 8$. The dotted line in the left panels are pure cosine functions $D(\Delta) = \langle D \rangle + \sqrt{2}\sigma_D \cos(2\pi f\Delta)$.

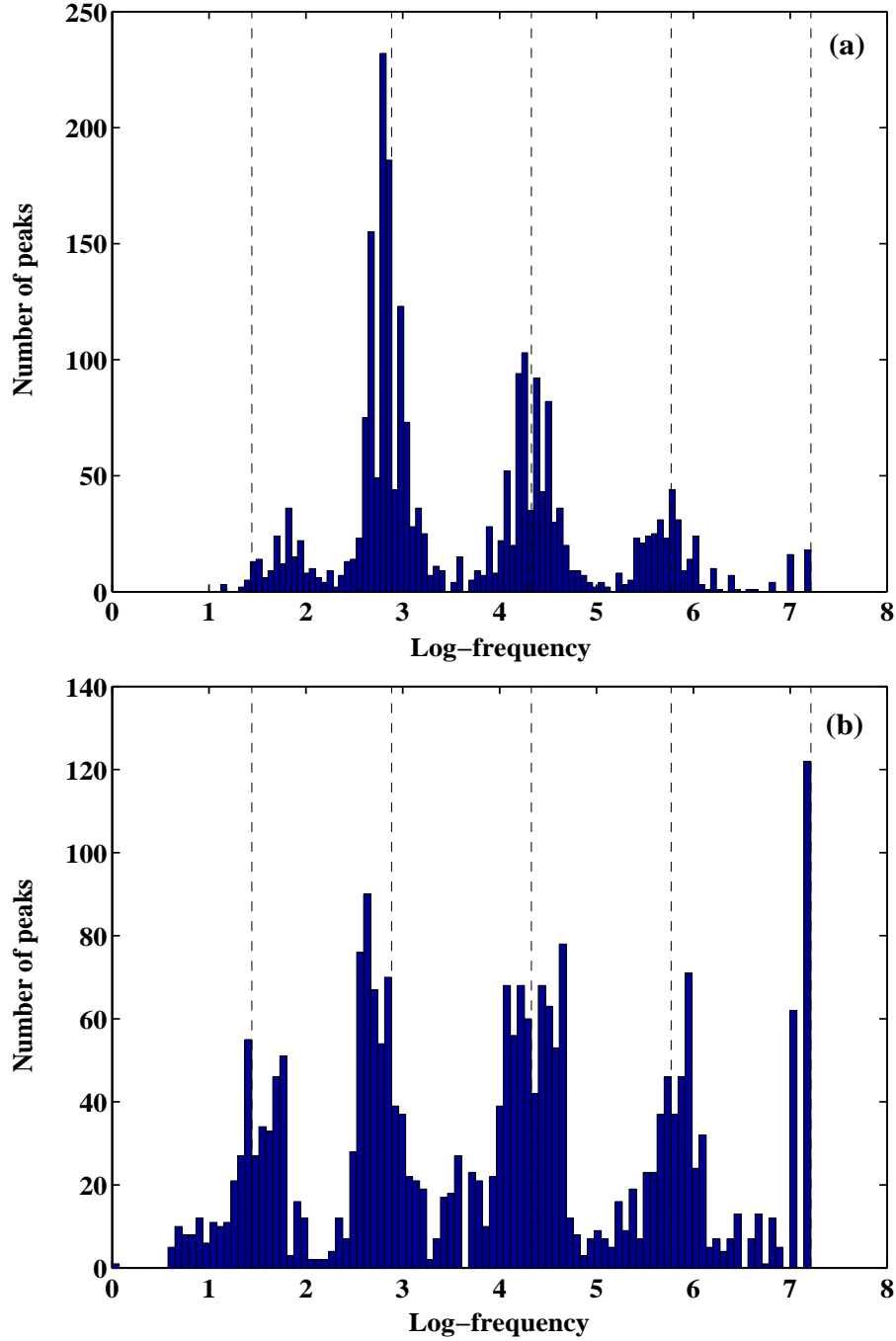


Figure 9: Histograms of all log-frequencies corresponding to (a) the most significant and (b) the second most significant Lomb peaks of all 2400 Lomb periodograms available from our analysis of 100 independent records by the 24 possible filters (spanning $N_L = 5 - 10$ and $M = 4 - 7$) used for each record. The vertical dashed lines correspond to log-frequencies equal respectively to $f_1 = 1.44$, $f_2 = 2f_1 = 2.89$, $f_3 = 3f_1 = 4.33$, $f_4 = 4f_1 = 5.77$ and $f_5 = 5f_1 = 7.21$, which correspond to increasing integer powers of a fundamental scale ratio exactly equal to $\gamma = 2$, through the relationship $f_1 = 1/\ln \gamma$.

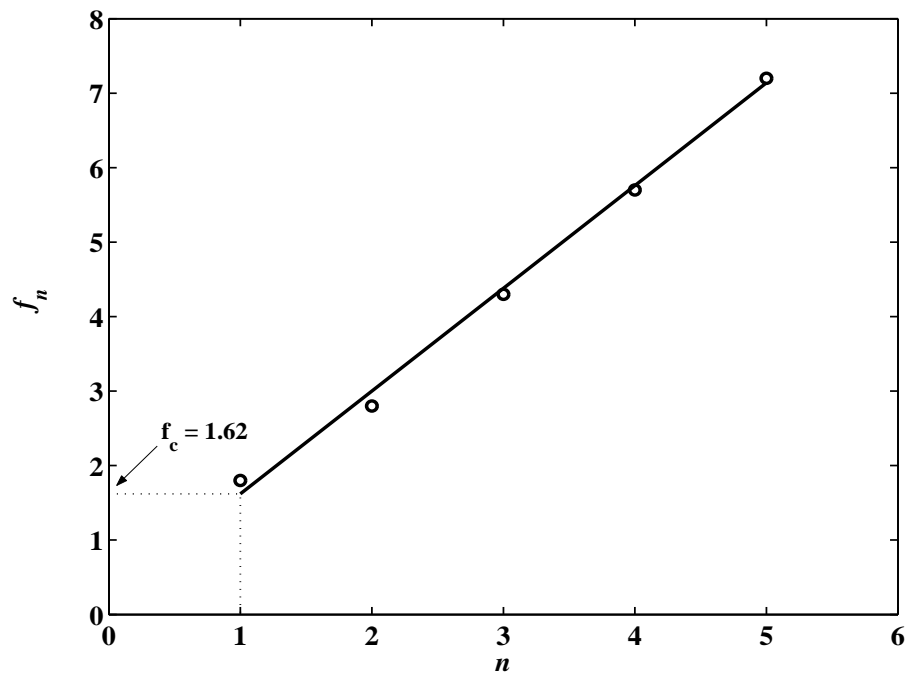


Figure 10: Value of the frequency measured at the n th maximum of the histogram shown in Fig. 9 as a function of the order n of the maximum. The straight line is a linear fit with the equation $f_n = n f_1$, where the adjustable parameter f_1 is found equal to $f_1 = 1.62 \pm 0.1$.

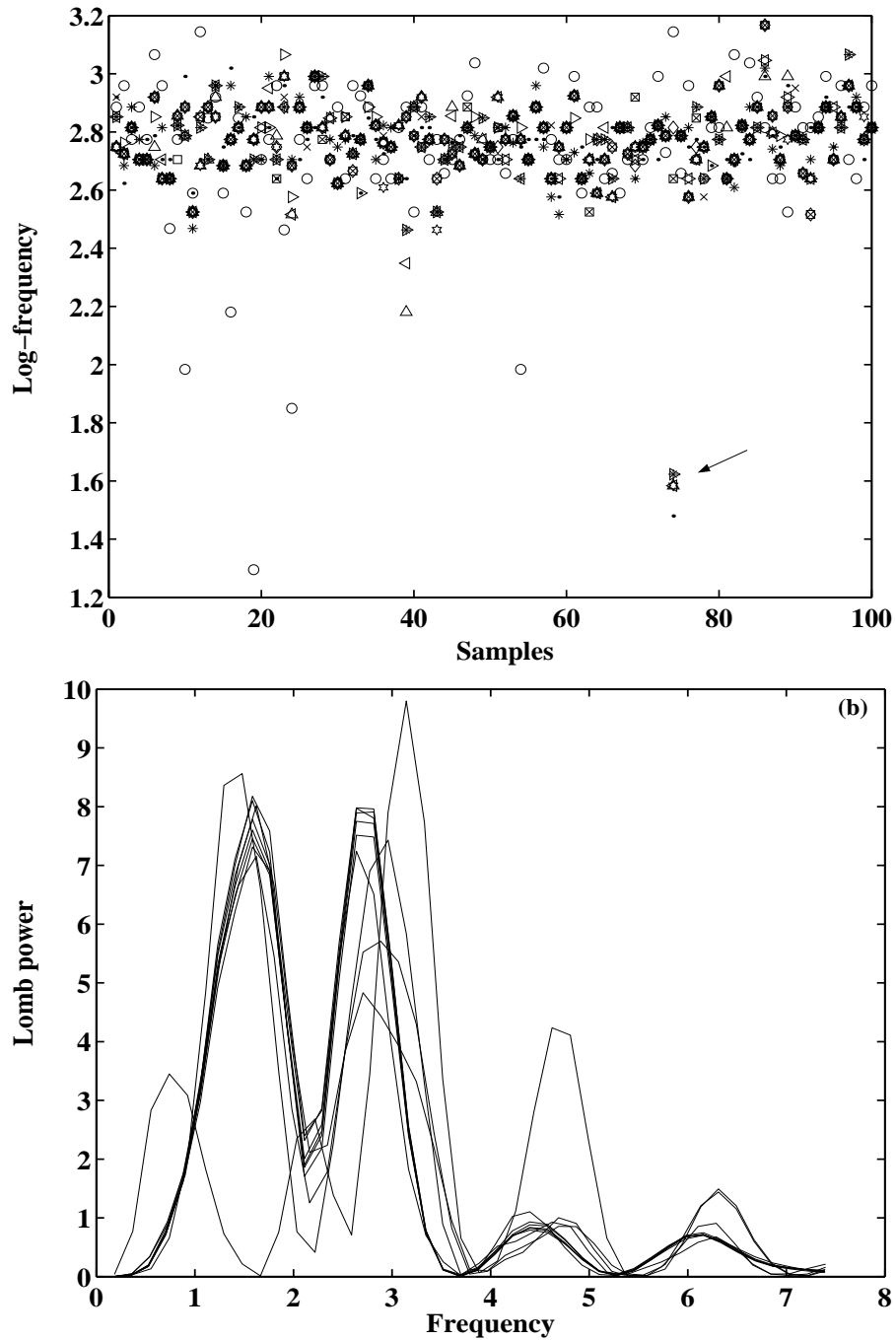


Figure 11: (a) Leading log-frequencies f of different records (numbered on the abscissa) calculated for different moment order q marked with different symbols ($q = 1$ corresponds to the open circles). The arrow indicates a large fluctuations of the best log-frequency occurring for the 74th record. (b) All the Lomb periodograms obtained for record 74.

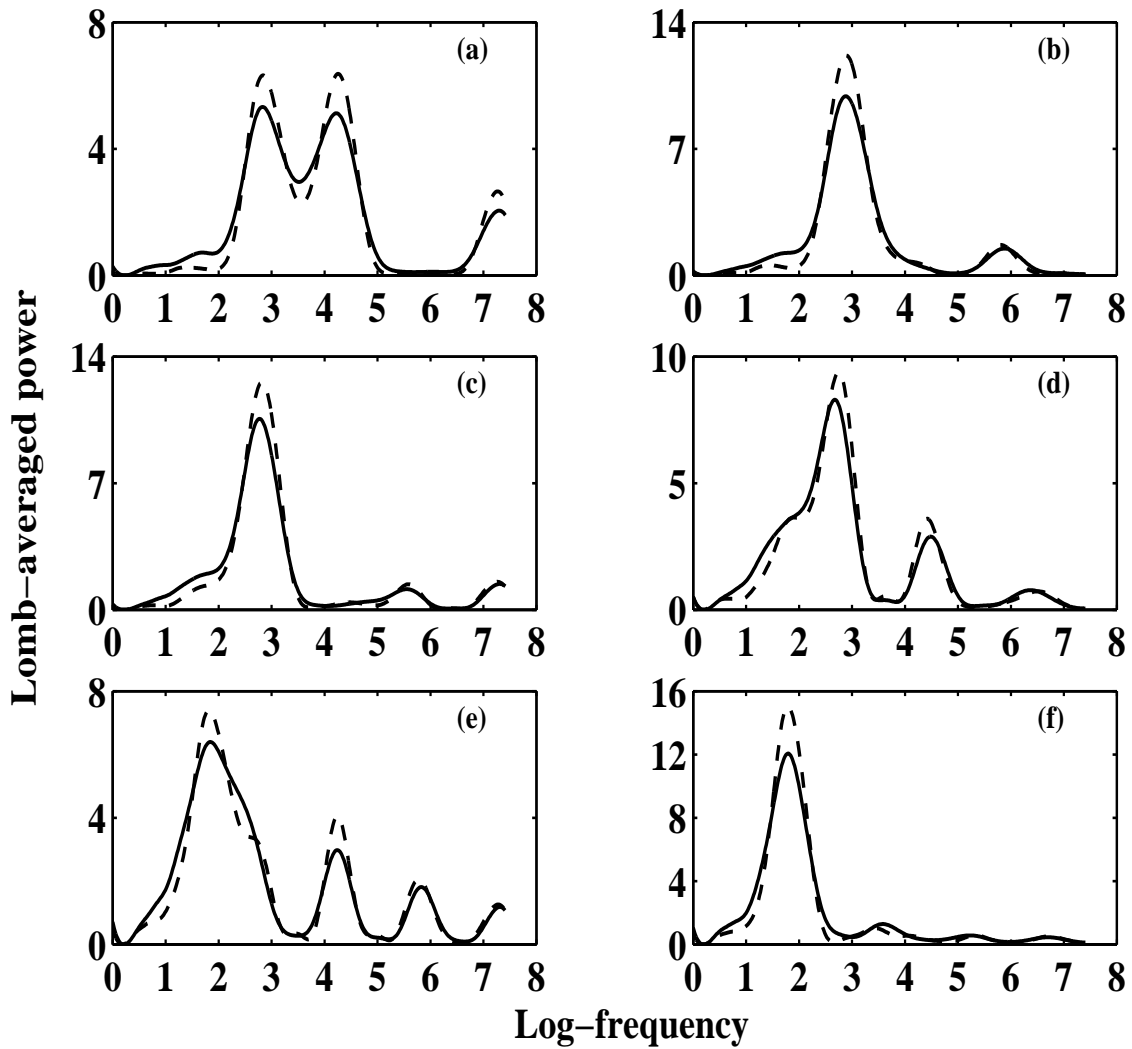


Figure 12: Lomb periodogram obtained by averaging over the $N = 100$ (solid curve), respectively the $N = 20$ (dashed line), records of length $L = 2^{17}$, respectively $L = 5 \times 2^{17}$. The order of the fitting polynomial of the Savitsky-Golay filter is fixed at $M = 4$, while N_L goes from 5 to 10 in panels (a) to (f).

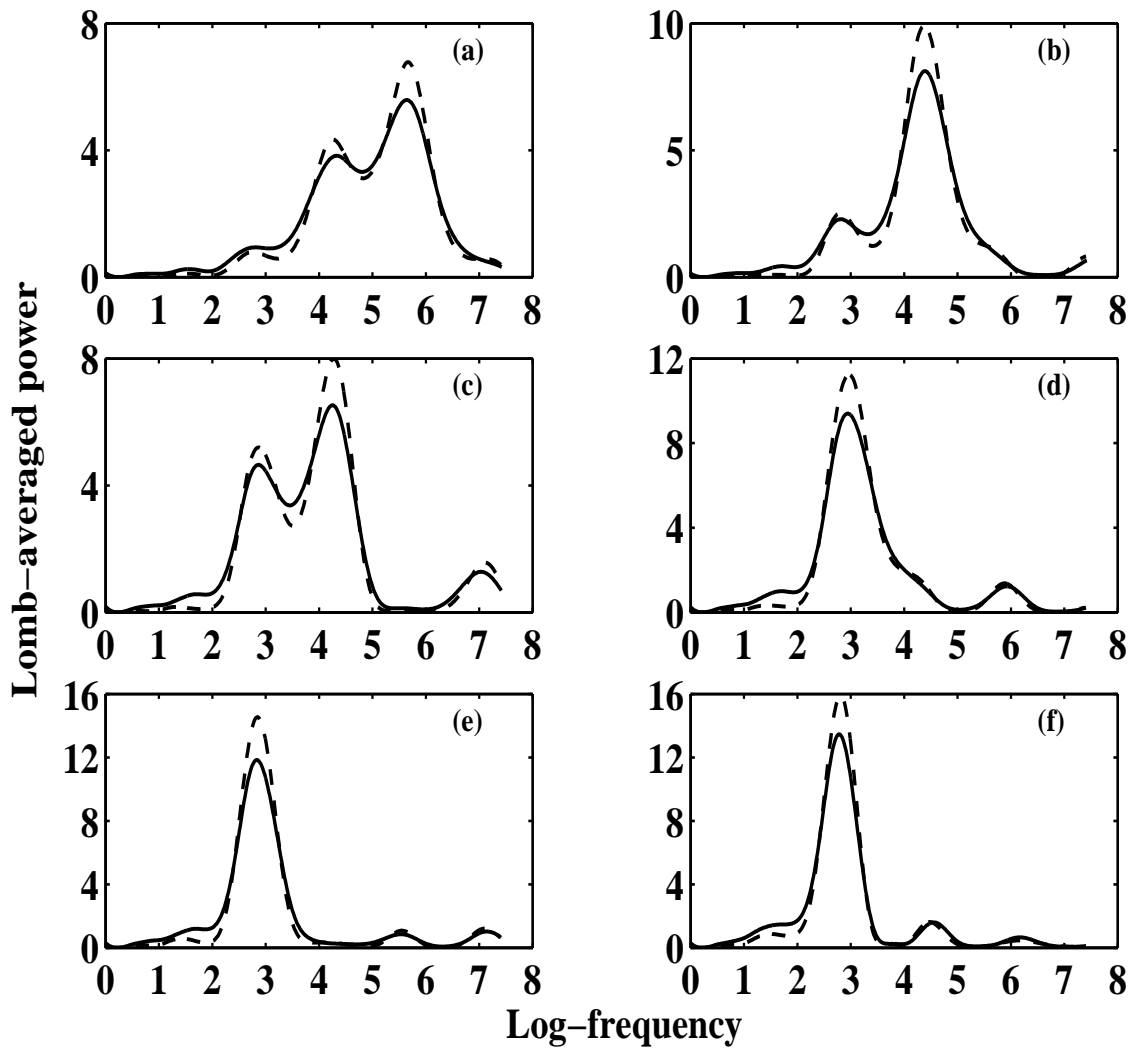


Figure 13: Same as Fig. 12 with the order of the fitting polynomial of the Savitsky-Golay filter fixed at $M = 5$.

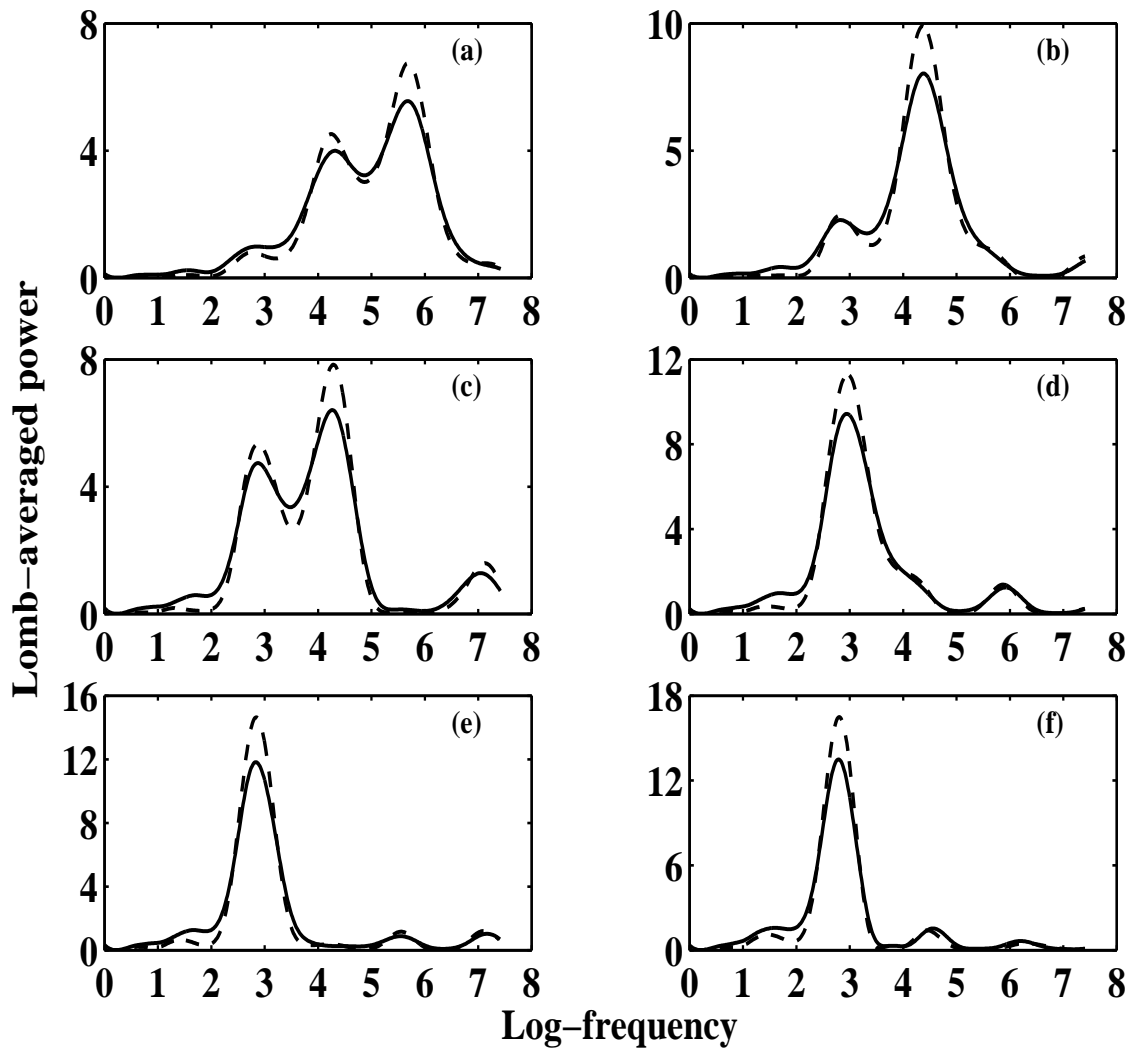


Figure 14: Same as Fig. 12 with the order of the fitting polynomial of the Savitsky-Golay filter fixed at $M = 6$.

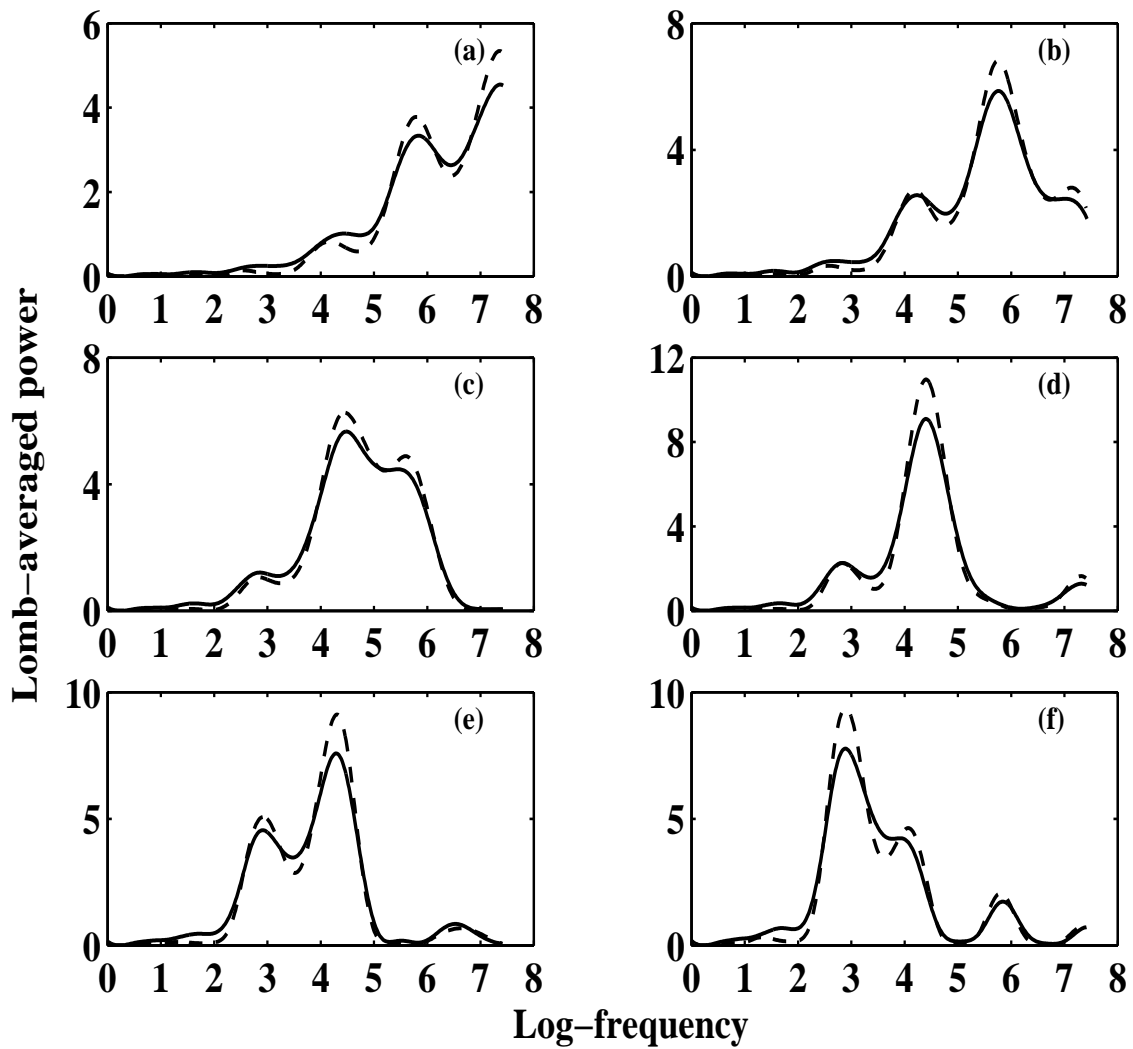


Figure 15: Same as Fig. 12 with the order of the fitting polynomial of the Savitsky-Golay filter fixed at $M = 7$.

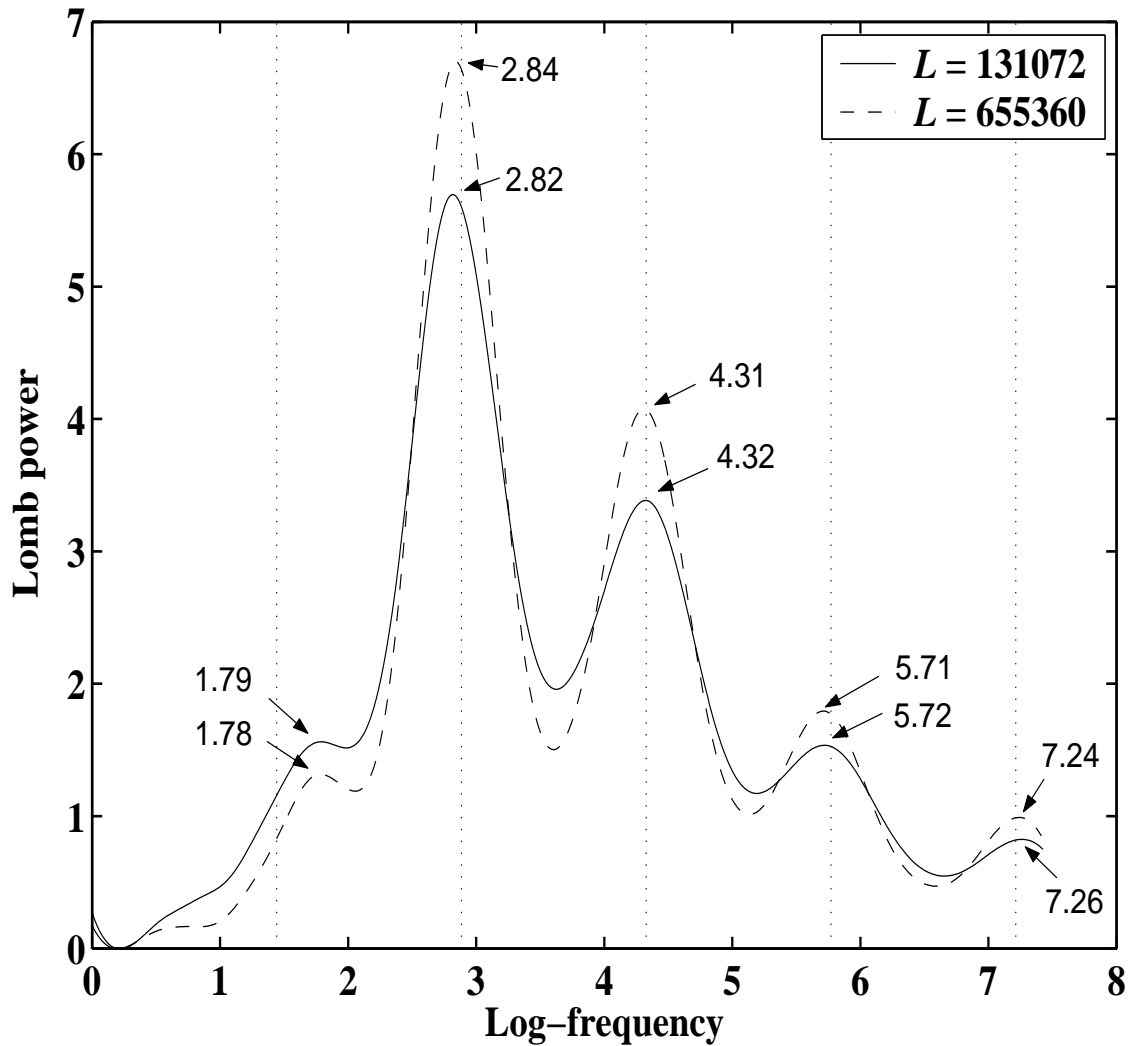


Figure 16: Average of all 2400 (continuous line) (resp. 480 (dashed line)) Lomb periodograms shown in Figs. 12-15 over all 24 filters and all records. The vertical dashed lines correspond to log-frequencies equal respectively to $f_1 = 1.44$, $f_2 = 2f_1 = 2.89$, $f_3 = 3f_1 = 4.33$ and $f_4 = 4f_1 = 5.77$. These values correspond respectively to increasing harmonics of a fundamental frequency $f_1 = 1/\ln \gamma$ associated with the scale ratio $\gamma = 2$.

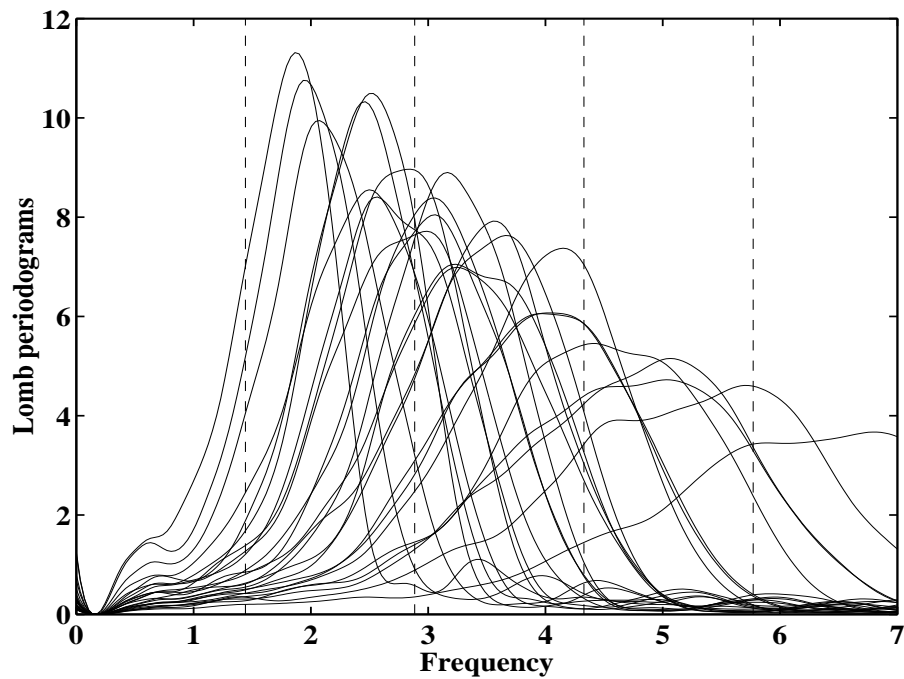


Figure 17: Lomb periodograms averaged over 100 samples of fractional Gaussian noises with the Hurst exponent $H = 0.99$, each set having 61 data points. One average Lomb periodogram is shown for each of the 24 values of the pair of parameters of the Savitsky-Golay filter: the order M of the fitting polynomial of the Savitsky-Golay filter ranges from 4 to 7, while N_L varies from 5 to 10. These average Lomb periodograms should be compared with Figs. 12-15.

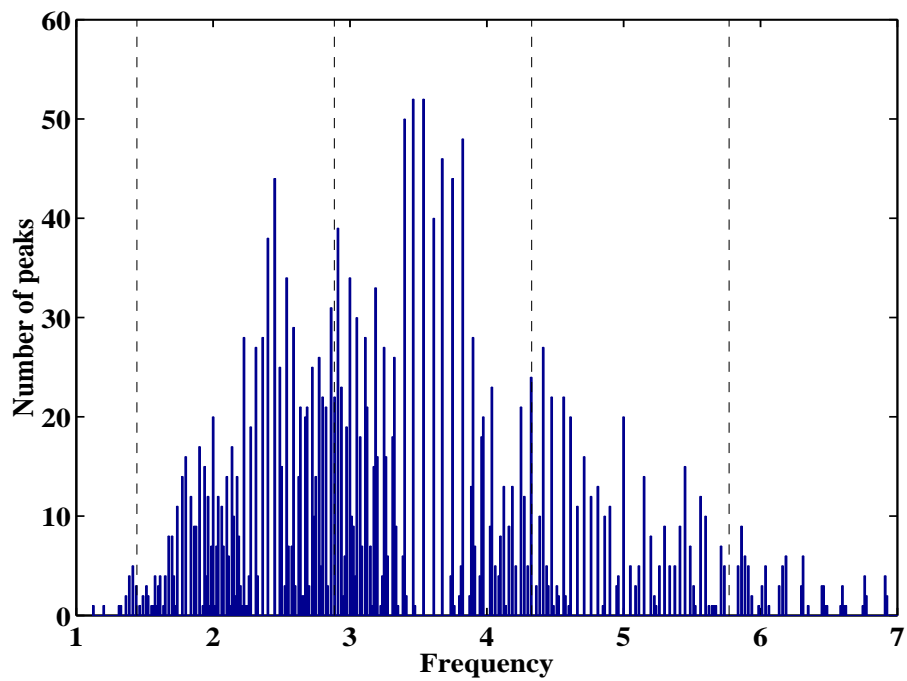


Figure 18: Histograms of all log-frequencies extracted from the largest peaks of the 2400 Lomb periodograms of synthesized fractional Gaussian noises with $H = 0.99$.